NORTHWESTERN UNIVERSITY

NUMERICAL SIMULATION OF MEASURED TIME DOMAIN REFLECTOMETRY SIGNATURES

A THESIS

SUBMITTED TO THE DEPARTMENT OF CIVIL ENGINEERING IN PARTIAL FULFILLMENT OF THE REQUIREMENTS

for the degree

MASTER OF SCIENCE

FIELD OF CIVIL ENGINEERING

by

Stéphane P. BORDAS

EVANSTON, ILLINOIS
December 1998

ACKNOWLEDGEMENTS

The author sincerely acknowledges his advisor Professor Charles H. Dowding, for his guidance and support throughout his research.

The author also wishes to extend his thanks to the members of the committee who reviewed this report:

Professor Richard J. Finno, who has instructed the majority of the author's classwork providing him with a multitude of knowledge,

Professor William L. Kath, who, in addition to writing the finite-difference code spent numerous hours advising the author on the numerical aspects of his work.

Special thanks is addressed to the graduate geotechnical group for their support throughout the author's studies at Northwestern.

ABSTRACT

Experimental Time Domain Reflectometry (TDR) data obtained from the field are compared with numerical simulations using a finite-difference solution of the transmission line equations. The model simulates transmission of a voltage pulse along a lossy coaxial cable where deformities on the cable, such as crimps and shears, are represented by capacitive discontinuities in the transmission line. Three reflection phenomena were studied in the field. The first was the increase in width and decrease in amplitude of a reflection as deformations within close proximity to each other but located at large distances from the source. These three field experiments were simulated with the model and comparisons were made to assess the model's ability to predict known behavior.

Results from the field data show a linear increase in reflection width with increasing propagation distance and an exponential decrease in reflection amplitude with increasing distance. A study of multiple discontinuities shows that upstream reflection amplitudes in excess of 100mρ will begin to influence a downstream discontinuity by reducing the downstream reflection amplitude. Studies of two or three shear discontinuities with a 1.5m separation distance resulted in no measurable changes in reflection caused by addition of the upstream shear discontinuities.

After the field data were collected, the model was calibrated with the measured reflection data for single discontinuities in a Comm/Scope P-3 75-875CA coaxial cable. Resistance was found by matching increasing crimp width with distance between 1 and 30m and 1 and 50m. A 12mm wide 120pF capacitive discontinuity best related modeled and measured crimps 12mm wide and 7.2mm deep at 51m and a 6mm wide 150pF capacitive discontinuity best related a 7.5mm shear displacement at 45m. With these calibrations, the model was able to predict known amplitudes to within 4mp of the measured values for single discontinuities up to distances of 94m. Simulations of the influence of an upstream crimp reflection resulted was a 72mm crimp. However, the influence of an upstream shear on a downstream crimp was detected by the code that showed a slight decrease in amplitude, yet much smaller than the measured data. These

results suggest the model is less sensitive to multiple discontinuities than observed in the field.

LIST OF FIGURES

LIST OF SYMBOLS

ROMAN LETTER SYMBOLS

C	capacitance	Farads	(F)
G	conductance		(Ω^{-1})
I	current intensity	Amperes	(A)
L	inductance	Henrys	(H)
Pf	picofarad		
R	resistance	Ohm	(Ω)
R_{inner}	cable inner conductor radius	Meters	(m)
R_{outer}	cable outer conductor radius	Meters	(m)
T	time	Seconds	(s)
T_r	rise time	Seconds	(s)
V	voltage	Volts	(V)
V_{prop}	propagation velocity	Meters per second	(m/s)
Z	impedance	Ohms	(Ω)
Z	length coordinate	Meters	(m)
Z_0	characteristic impedance	Ohms	(Ω)

GREEK LETTER SYMBOLS

ΔC	change in capacitance	Farads	(F)
Δl	length of rise time	Seconds	(s)
ΔZ	elemental length	Meters	(m)
ε_0	permittivity of vacuum	Farads per meter	(F/m)
ε_{rel}	relative permittivity	Farads per meter	(F/m)
π	pi		
ρ	reflection coefficient		
μ_0	permeability of free space	Henrys per meter	(H/m)
mρ	millirhos		

TABLE OF CONTENTS

1. INTRODUCTION

This thesis summarizes the research undertaken at Northwestern University to compare measured time domain reflectometry (TDR) voltage reflections with numerical simulations using a finite difference model of a deformed transmission line. The purpose of this work is to numerically simulate voltage reflections from multiple discontinuities in a lossy coaxial cable to determine the effects of multiple discontinuities at variable distances on the reflected signature. This project was performed in three stages. First, TDR reflection data were collected along a 530m long coaxial cable. Second, appropriate finite difference model was selected to simulate the experimental TDR reflections. Third, the model was calibrated with field data from single discontinuities in order to test its ability to simulate reflective interaction of multiple discontinuities.

If field reflections can be accurately replicated with a numerical model, it is possible to predict the amount of deformation the cable has undergone by interpreting the amplitude and width of the reflection the deformity produced. Previous work by Kroll (1996) simulated voltage reflections in a lossy finite-difference model by modifying resistance as a function of dominant frequency. However, those frequency dependent loss calculations were not stable after reflection. Thus, only propagation to and slightly after reflection was studied. Since instruments measure the signal after a complete round trip, source-reflection-source, this approach was insufficient. This new study accounts for energy losses in the cable through a Fourier Transform approach (Kath, 1998), where frequency dependent losses are applied in the frequency domain and then transformed back to the physical or time domain. Incorporation of resistance allows the reflection to change in width and amplitude with distance resulting in reflections with behavior similar to reflections measured in the field.

This report is arranged into six chapters and a number of appendices. Chapter 2 describes the background behind transmission line theory, the terminology used and the methods for measuring reflection signatures. Chapter 3 summarizes reflection signatures from field tests of long cables. Chapter 4 describes the numerical approach to modeling TDR reflections and its calibration to field data. Chapter 5 compares the modeled reflection signatures to the measured field signatures. Finally, Chapter 6 presents

conclusions and recommendations on the accuracy and behavior of the Fourier transform approach to modeling the propagation and reflection of TDR pulses. The appendices present the details of the work. Appendix A presents the source code in FORTRAN. Appendix B presents input data and results from an example run to allow a check for future users.

2. BACKGROUND

Time Domain Reflectometry (TDR) has been employed to measure rock deformation since the early 1980's and is now being extended to measure soil deformation (Dowding, Pierce 1994). Coaxial cables are grouted into a rock or soil mass, and localized movement along joints or shear bands will deform the cable, which changes TDR pulse reflection signatures. Increasing reflection amplitudes correspond to increasing cable deformation.

Coaxial cables provide a one-dimensional propagation path for the voltage pulse or electromagnetic wave, which is governed by Maxwell's equations of wave propagation through dielectric media. A coaxial cable is composed of an inner and outer conductor between which is placed a dielectric material, as shown in Figure 2-1a. As shown in Figure 2-1b, this structure is usually modeled by a succession of circuits of elemental length, Δz. Each of these elements is composed of a given association of capacitance (C), inductance (L), conductance (G) and resistance (R) that can be defined as follows:

Capacitance per unit length (C): voltage difference created between the inner and outer conductors;
Inductance per unit length (L): magnetic field induced in one conductor by the flowing current in the other;
Conductance per unit length (G): dielectric conductivity;
Resistance per unit length (R): energy absorption by the two-conductor system.

From these properties, the characteristic impedance Z_0 of the cable can be defined as:

$$Z_0 = \sqrt{\frac{L}{C}} \tag{2-1}$$

The impedance for each elemental circuit also can be defined as the ratio of the voltage V to the current I:

$$Z(z) = \frac{V(z)}{I(z)} \tag{2-2}$$

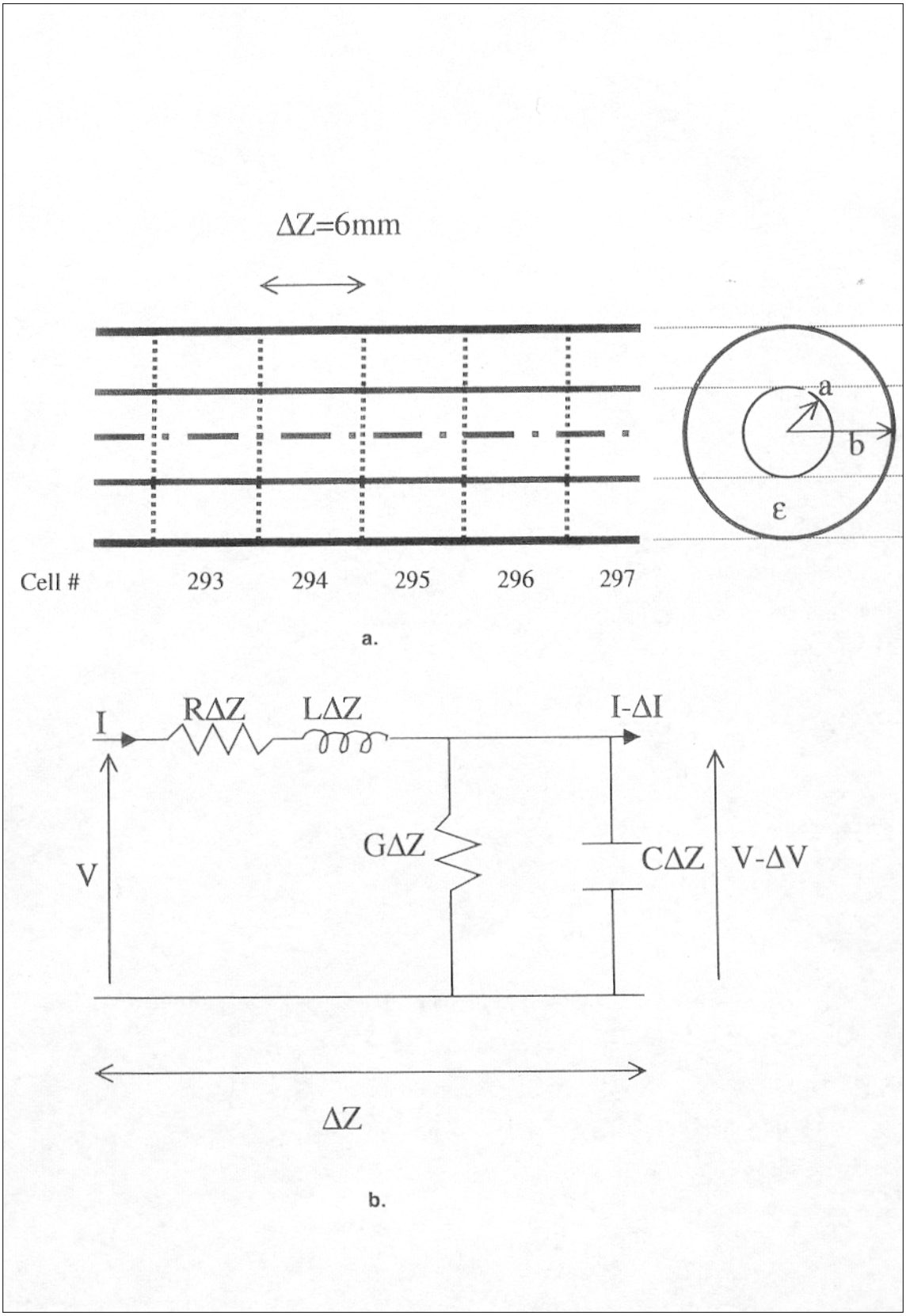

Figure 2-1
Section of a coaxial cable and equivalent lumped circuit

The reflection coefficient, ρ, is used as a means to measure reflection amplitudes of the TDR voltage pulses as shown in Figure 2-2. It is defined as the ratio of the reflected voltage, ΔV, to the incident voltage V_0.

$$\rho(z) = \frac{\Delta V}{V_0} \tag{2-3}$$

The magnitude of reflection ratio is described as rhos (ρ). Where one millirho is equal to 0.1%. As propagation distance increases, reflection amplitude decreases and width increases due to lengthening of the rise time as shown in Figure 2-3. This smearing of the wave front is known as dispersion and results from energy losses from resistance in the coaxial cable. These losses are called “skin effects” (Taflove, 1996) and play an important role in describing the behavior of a propagating wave.

Two differential equations can be employed to describe the variation of voltage and current over numerous space and time increments or cells in a simulated coaxial cable. Voltages and currents are function of both time and space (t and z). The first equation for one-dimensional wave propagation gives the space derivative of the current: (Miner, 1996)

$$\frac{\partial I}{\partial z} = -C\frac{\partial V}{\partial t} - GV \tag{2-4}$$

The second equation expresses the space derivative of the voltage as follows: (Miner, 1996)

$$\frac{\partial V}{\partial z} = -RI - L\frac{\partial I}{\partial t} \tag{2-5}$$

Equations (2-4) and (2-5) are the two fundamental equations that will be employed to calculate voltage and current along a coaxial cable. They are more commonly used in electrical engineering than the second order wave equations and will therefore be used in this simulation. Boundary conditions are built in explicitly and do not need to be enforced (Taflove 1996).

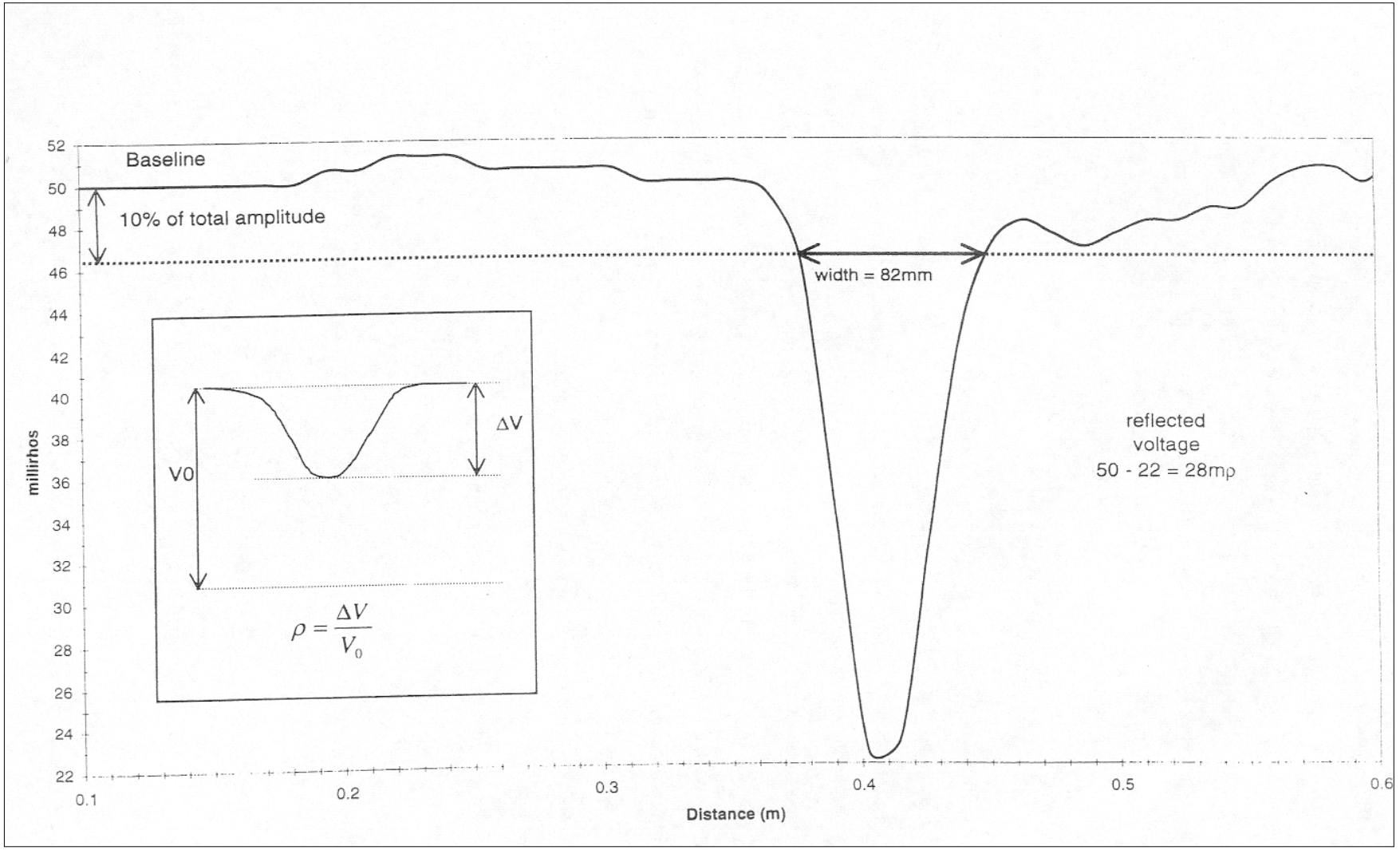

Figure 2-2
Measurement of a crimp at 6m

Reflection shown in Figure 2-3b is produced when changes in the geometry of the cable, such as a reduction in diameter, create a change in its electrical properties. The pulse reflects off these discontinuities and returns to the source. Reflections can also be caused by changes in the dielectric material or by abrasions on the outer conductor. However, the focus of this investigation will be discontinuities caused by changes in the cable's geometry. Field pulses are launched and recorded by a Tektronix 1502B TDR cable tester in this study. It launches multiple, one-volt signals with a 200 picosecond rise time along the cable and records the reflections that return to the source (Tektronix, 1975).

Figure 2-2 shows a typical reflection recorded by the cable tester. The discontinuity was caused by shearing the cable 6 meters from the upstream end nearest the pulser. The reflection amplitude is measured from the baseline to the trough of the reflection. Figure 2-2 shows a baseline of 50mρ and a trough of 22.6mρ producing a reflection amplitude of 27.4mρ. In order to reduce errors read from small changes near the endpoints of the reflection, the reflection width is arbitrarily measured at 10% of the total amplitude, that is 2.74mρ. Subtracting 2.74mρ from the baseline of 50mρ produces endpoints with amplitudes of 47.3mρ. Therefore, when moving from left to right, the width is measured from the start at 47.3mρ until the amplitude once again reaches 47.3 mρ. As shown in Figure 2-2, the width of the crimp reflection a 6 meters is measured as 82mm wide.

All the field data that will be presented later on were imported, viewed and analyzed using **N**orthwestern **U**niversity **T**DR **S**ignature **A**nalysis (NUTSA) software (Huang et al, 1993). This program gives the coordinates of each data point on the screen and allows accurate determinations of the width (mm) and amplitude of the reflection (mρ).

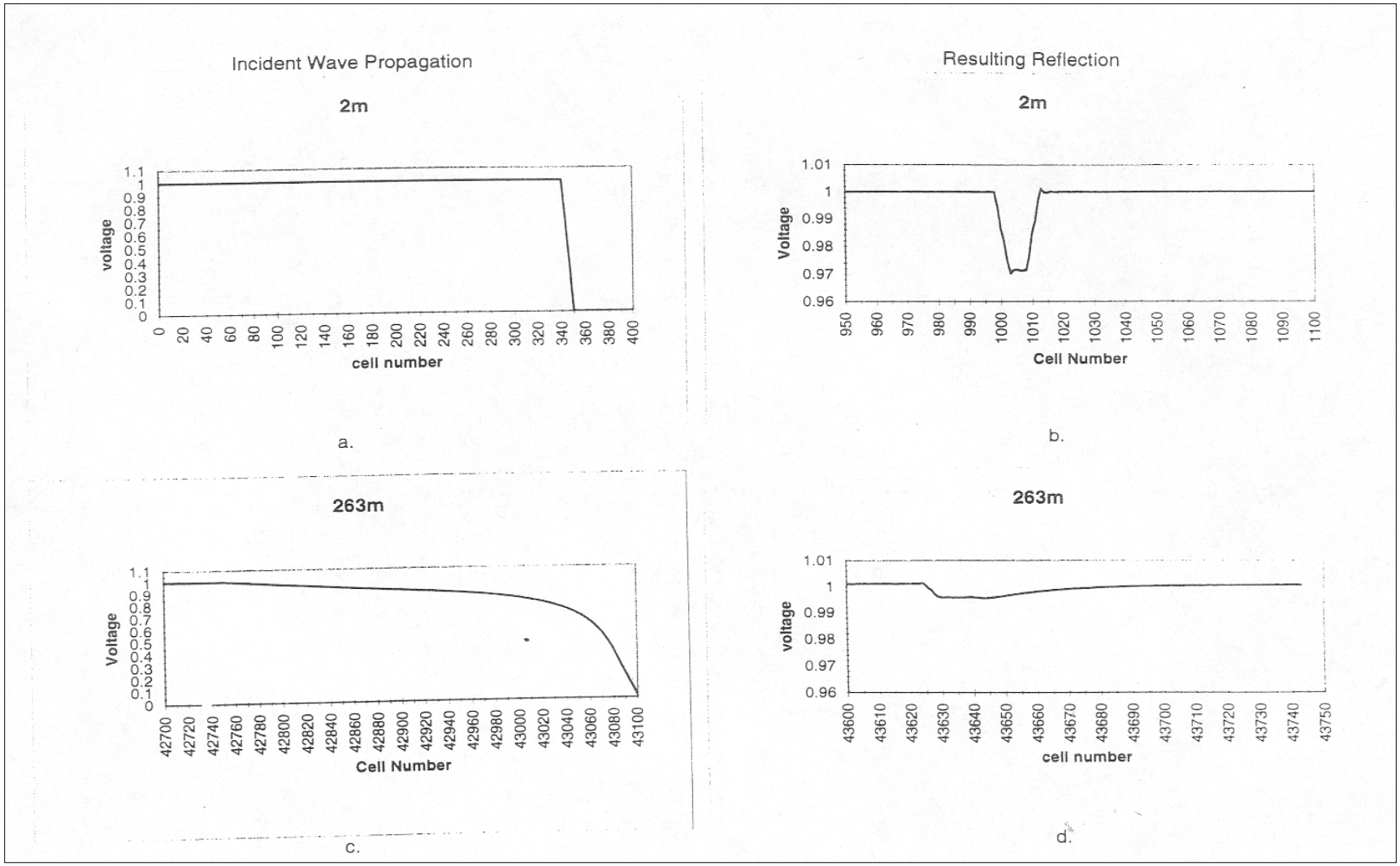

Figure 2-3
Comparison of the incident wave at 2m and 263m and its corresponding reflection signatures

FIELD TEST DATA

A 530m long, 22.2mm diameter solid aluminum coaxial cable similar to that used to monitor rock displacement and subsidence over abandoned mines, was deformed by Pierce et al (1994) at varying distances to gather voltage reflection data. Crimps and shears were placed at increasing distances up to 527m and their voltage reflections were measured.

As described by Pierce et al (1994), crimp deformations are typically placed at set intervals prior to installation of the cable to serve as distance markers. They are created by clamping the cable to a specified diameter with a pair of standard vice grips. In this study they are 12mm wide and reduce the cable diameter from 22.5 to 15mm. To generate crimps of larger width, the cable is clamped adjacent to the previous crimp. Widths of crimps will therefore be multiples of 12mm.

Single shear deformations were created by the shear box shown in Figure 3-1a. This device produces single shear deformities, which would be produced in the field by dislocations along a single sliding rock joint or soil shear band. The shearing occurs over a 2mm width and axial displacements are caused by turning the screw on the left. Figure 3-1b presents photographs of both a shear deformation and a crimp deformation.

3.1. Single deformities

Figure 3-2a,b,c shows reflections from the TDR pulser made by a 7.5mm shear displacement at 45m, 92m, and 265m respectively. Figure 3-2d,e,f shows the reflections for a single crimp a 6m, 94m, 263m respectively. The first deformation was placed at a distance of 265m from the pulser and its reflection was measured. Subsequent deformations were placed at decreasing distances from the pulser until the last and closest reflection was placed at 6m. With this sequence of events, no upstream deformations interfered with downstream reflections. Three observations can be made from Figure 3-2. First, the width of the reflection increases with distance. Second, the amplitude of the reflection decreases with distance. Both of these changes in the reflection result from the dispersion or lengthening of the signal front that results from energy losses as the signal

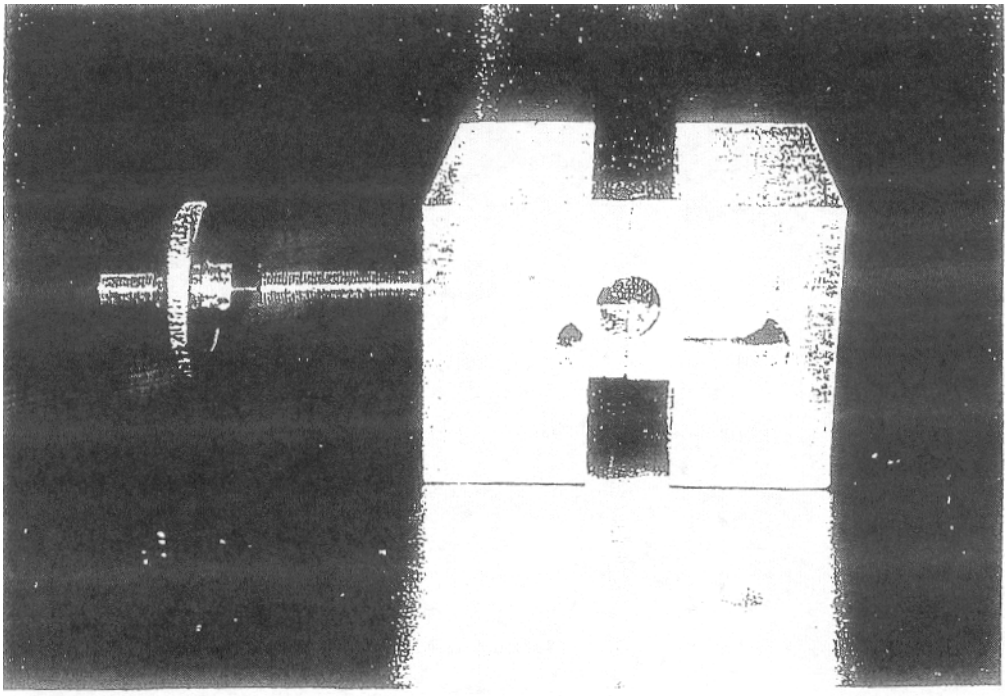

a.

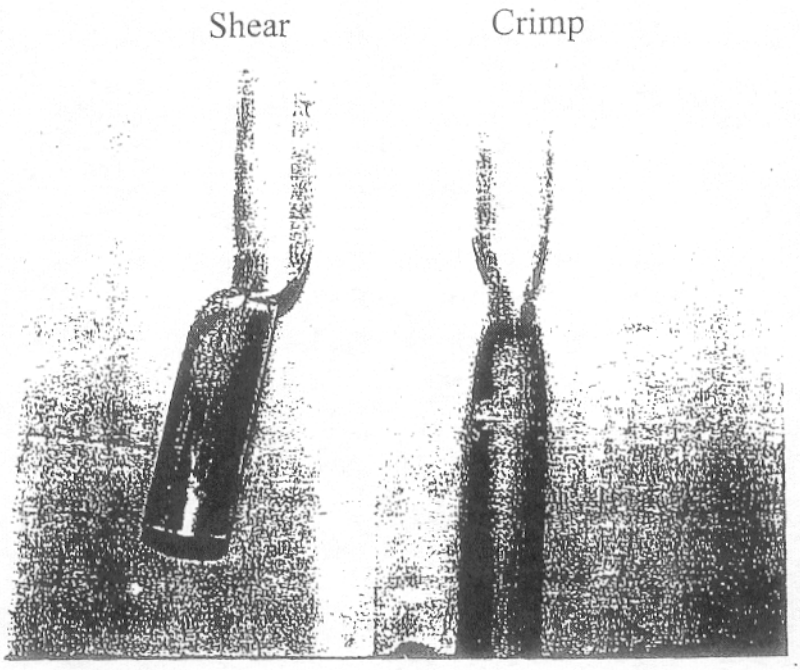

b.

Figure 3-1: a. Photograph of shearing apparatus. b. Photograph of deformed cable caused by a shear deformation (left) and a crimp deformation (right). (After Pierce et al, 1994).

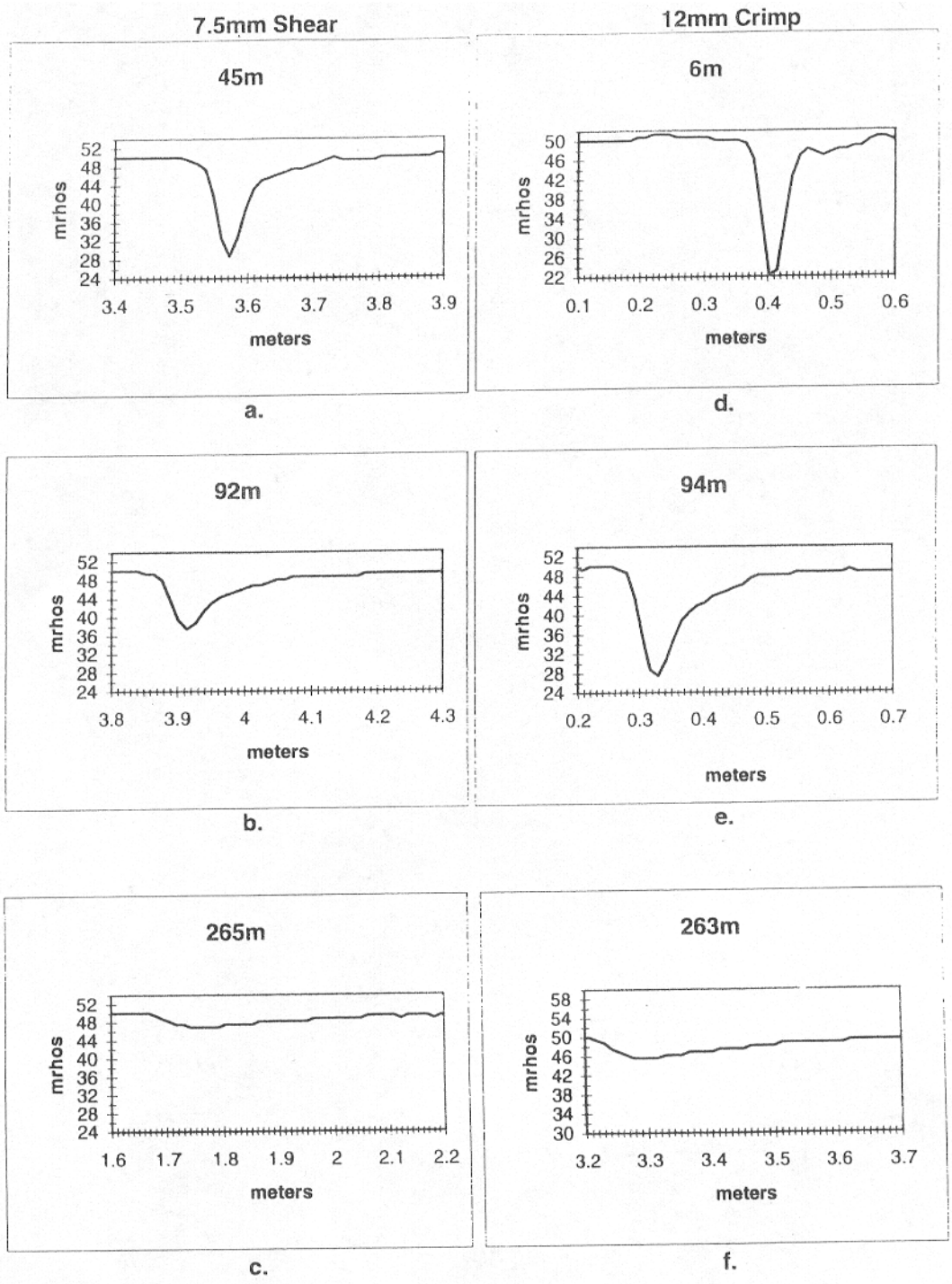

Figure 3-2
Field shear and crimp reflections at increasing distances.

travels down the cable. Third, at comparable distance the thinner shears produce smaller amplitude reflections.

Figure 3-3 shows that a 3:1-linear relationship exists between crimp induced reflection width and distance traveled over a distance of 100m. Previous work by Pierce et al (1994) describes exponential relationship between amplitude and transmission distance for shears for travel distances up to 500m, as shown in Figure 3-4b. Figure 3-4a plots reflection amplitude versus distance for the nine crimps shown in Figure 3-3. At short distances, it shows a more random relationship between signal amplitude and transmission distance. However, given that an exponential relationship does exist for long travel distances, the position of the data points does allow for the possibility of an exponential curve fit within the given data points.

3.2. Two Deformities at Large Separation Distances

It is important to validate the model for both single and multiple deformities. Interaction between multiple deformities is most important as multiple deformities are likely. Once the model is validated for simple single interactions, it can then be employed to predict likely amplitudes resulting from more complex but untested combinations that occur in the field. The most simple interaction is that between two shears or a crimp and a shear. It is important to evaluate how the downstream reflection coefficient changes when the deformity of an upstream shear increases.

To model a simple two-deformity interaction, the effect of an upstream shear on a downstream crimp was measured. Figure 3-5a presents the reflected signal of the shear as the relative shear of the 22.2mm diameter cable is increased from 5 to 16mm. Reflection amplitude is shown to increase with a slight increase in width. This slight increase in width agrees with the physical deformations in the cable since it begins to deform outside of the 2mm shear band as shearing increases. Figure 3-5b presents the measured downstream effect on the crimp.

After the upstream shear experiment was completed, an upstream crimp was increased in width. The change in its reflected signature as the width increased from 12mm to 60mm is shown in Figure 3-6a. Reflection width and amplitude increase as the crimp width increases. This also agrees with physical deformations in the cable since the

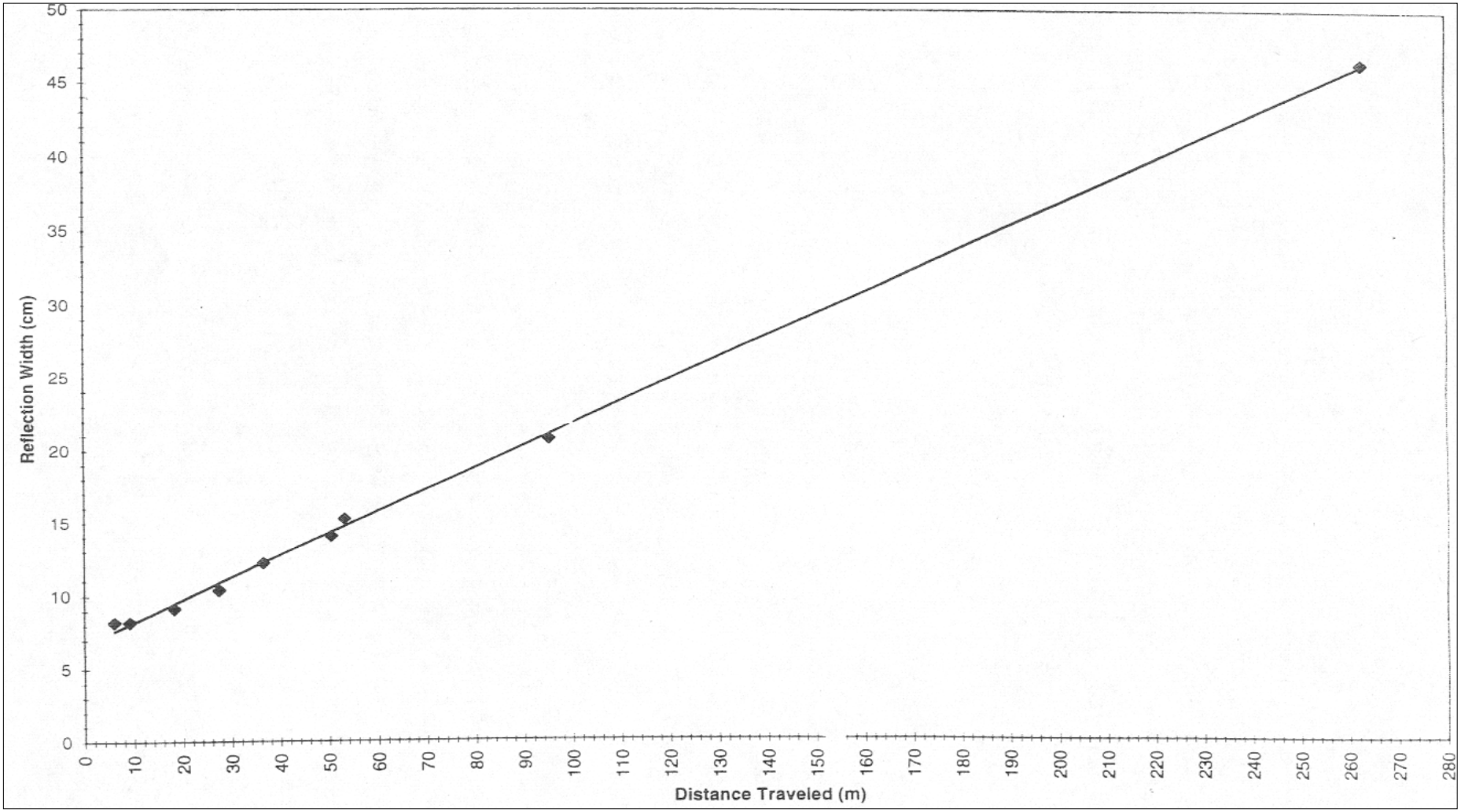

Figure 3-3

Measured reflection width produced by a single standard 12mm wide, 7.2mm deep crimp located at an increasing distance from the pulser.

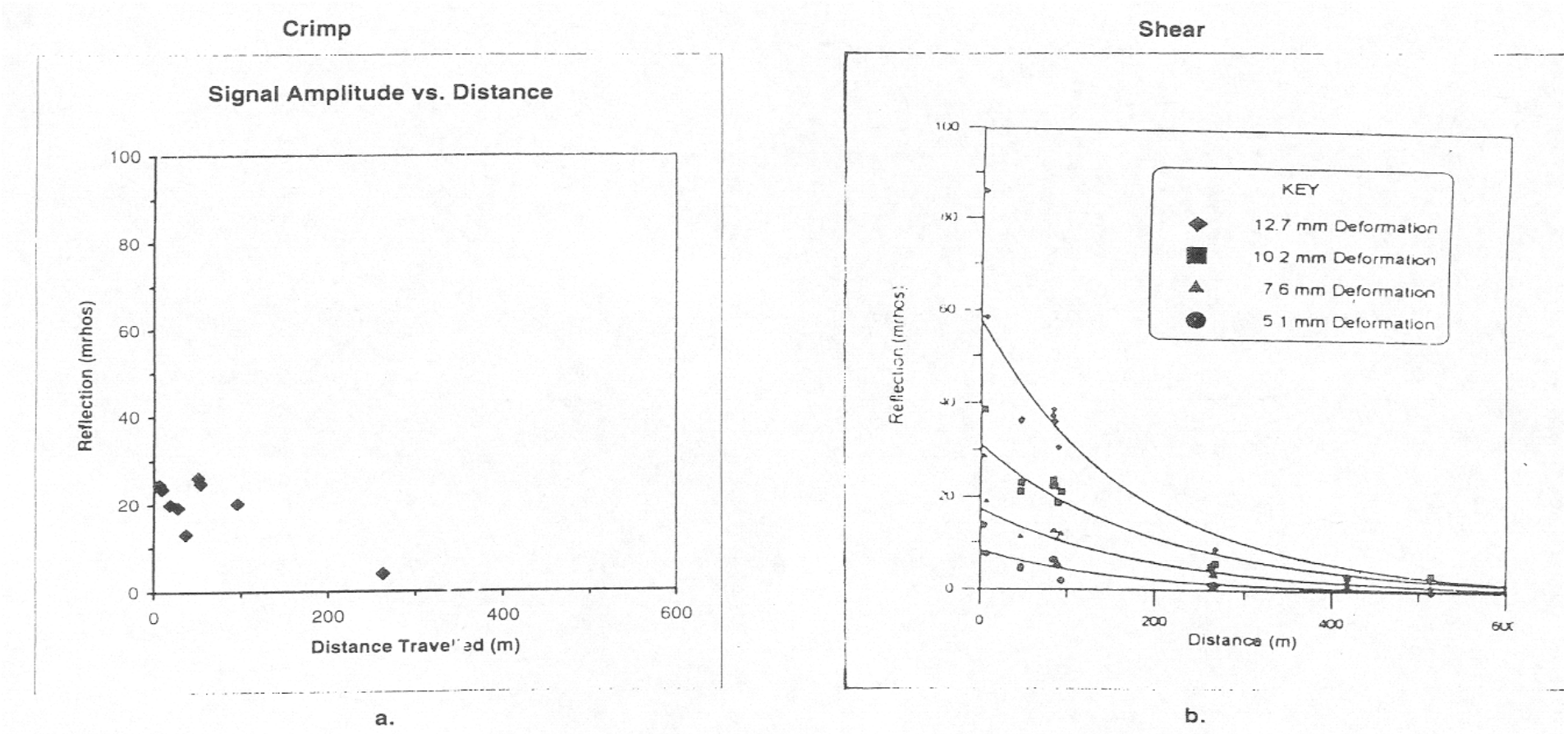

Figure 3-4: Comparison of amplitude vs. travel distance for a. single crimp (12mm wide) and b. shear displacements (2mm wide) (after Pierce et al, 1994)

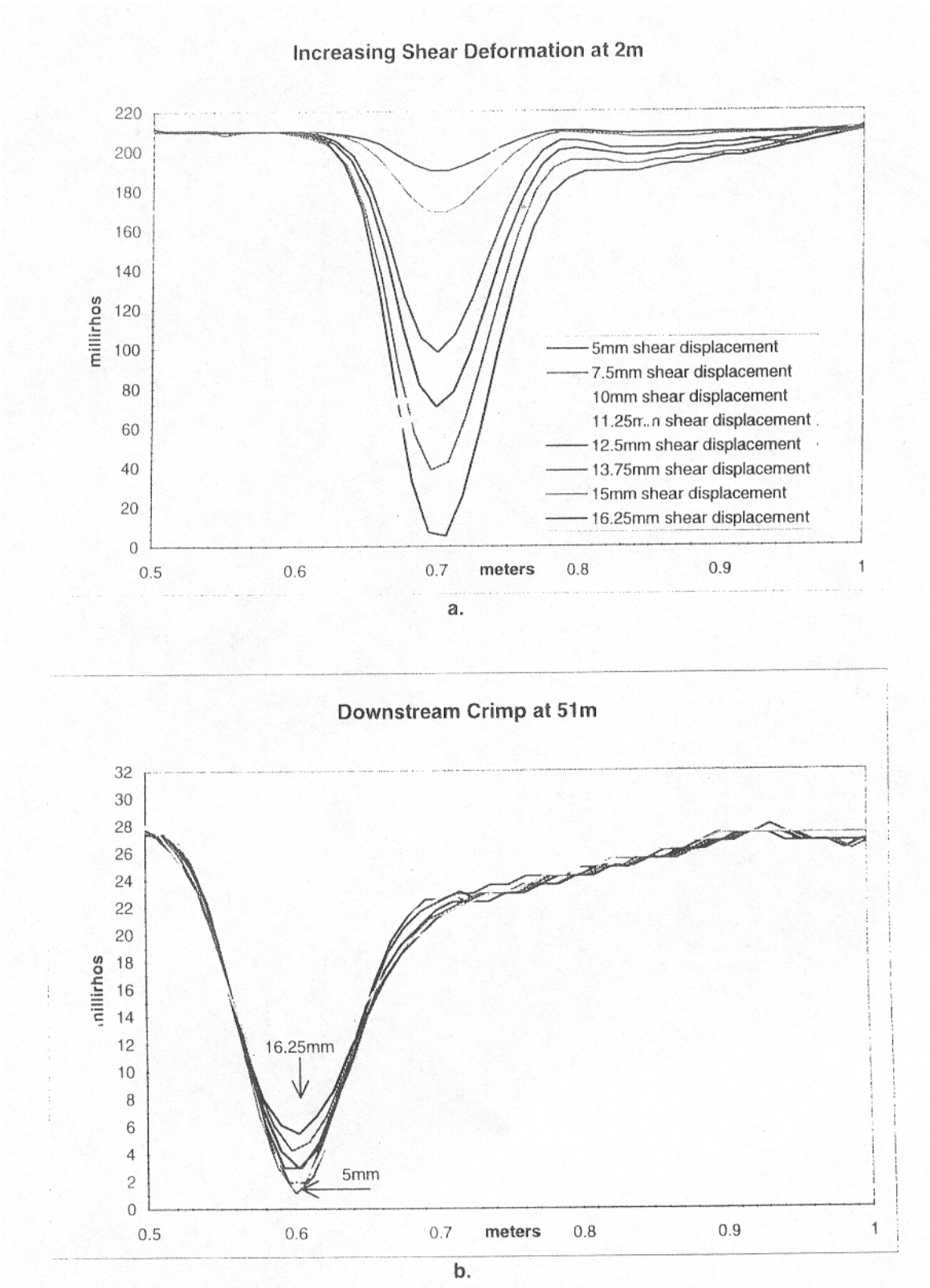

Figure 3-5: Effect of an increasing upstream shear reflection on a downstream crimp reflection.

deformation width is increasing. The effect on the downstream crimp is shown in Figure 3-6b. Comparison of Figure 3-5b and Figure 3-6b shows that there is a less downstream effect produced by increasing the width of the crimp than by increasing the shear displacement beyond 12mm.

These results show that increasing the shear deformity has a greater effect on downstream reflections than increasing the width of a crimp. Figure 3-6 shows that a 60mm wide, 7.2mm deep crimp did not affect the downstream crimp reflection. However, Figure 3-5 shows that an upstream shear 2mm wide with shear displacements greater than 12mm deep (almost twice that of the crimp) were necessary to produce more than a 1.4mρ change in the downstream reflection or a 5% change as shown in Figure 3-7. This influence results from the large reduction in diameter by shearing than by crimps. Thus changing more significantly the signal to be reflected by the downstream crimps.

3.3. Multiple Deformities at Small Separation Distances

To study the interaction of distant multiple shears within close proximity to each other, Pierce et al (1994) performed the following experiment. Two shears were placed 1.5m apart from each other at a distance of 95m and a similar set was placed at a distance of 263m. The experiment was conducted by first creating a 10mm shear displacement at 263m and recording its reflection data. Next, a shear was created 1.5m upstream from the original shear. Shear displacements were made in 2.5mm increments from 5 to 10mm. Reflection data were recorded at the end of each increment until the second shear deformation reached 10mm. The same procedure was repeated at 95m. Figures 3-8a and 3-8b show the results of the two experiments. The data show that at both 95m and 263m, there was essentially no loss in amplitude nor gain in width of the downstream reflection as the upstream reflection increased.

To investigate further interaction of distant but close deformations, a third shear was added 1.5m upstream of the second shear deformation at 95m. Reflection data were again measured at shear displacements of 5mm, 7.5mm and 10mm. The data are shown in Figure 3-8c. Once again, the third shear produced no noticeable effect on the other shear reflections. It should be noted that all three reflection amplitudes are not uniform in

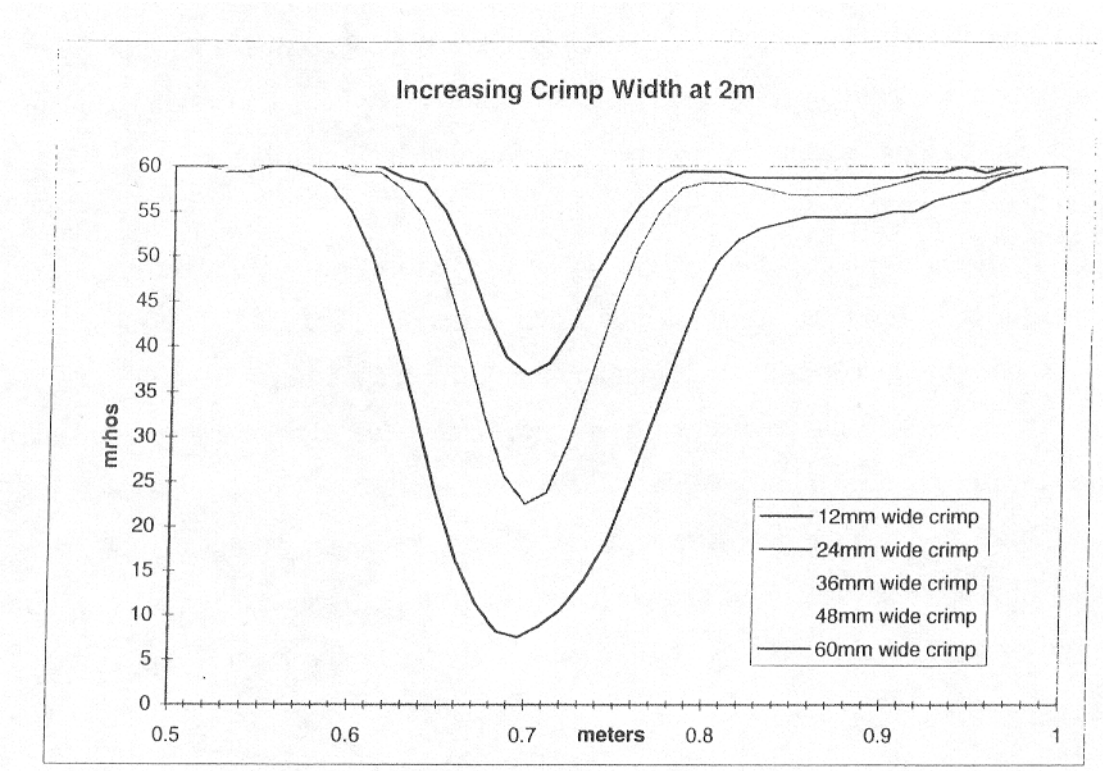

a.

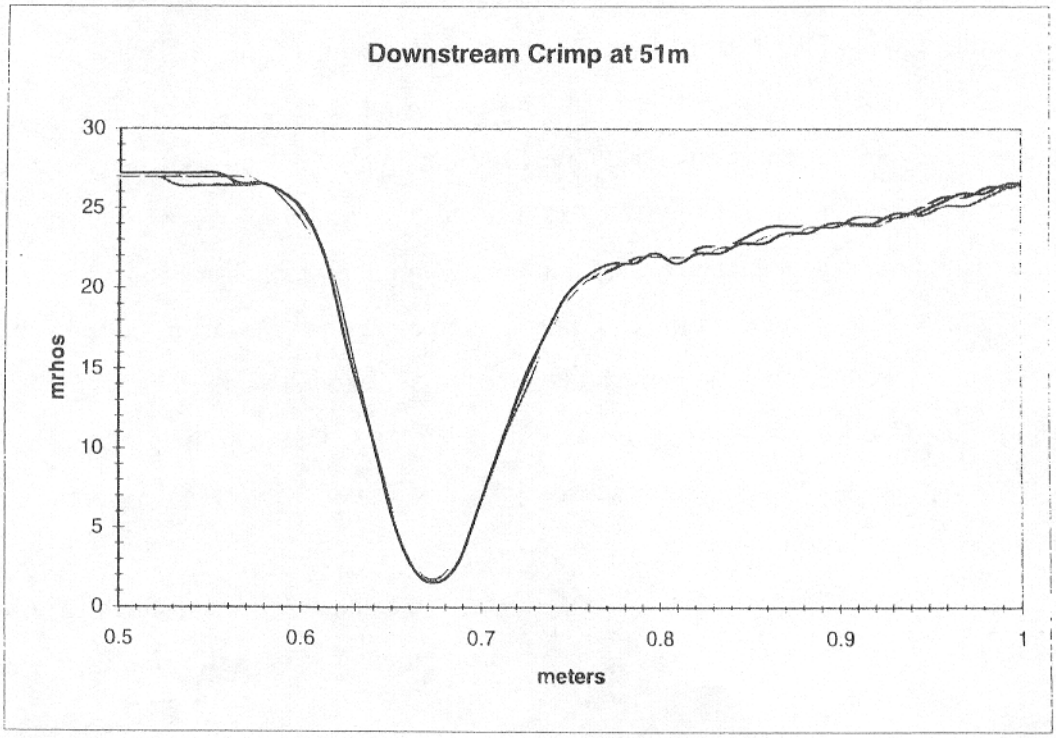

b.

Figure 3-6: Effect of a reflection from an increasing upstream crimp width on a downstream crimp reflection.

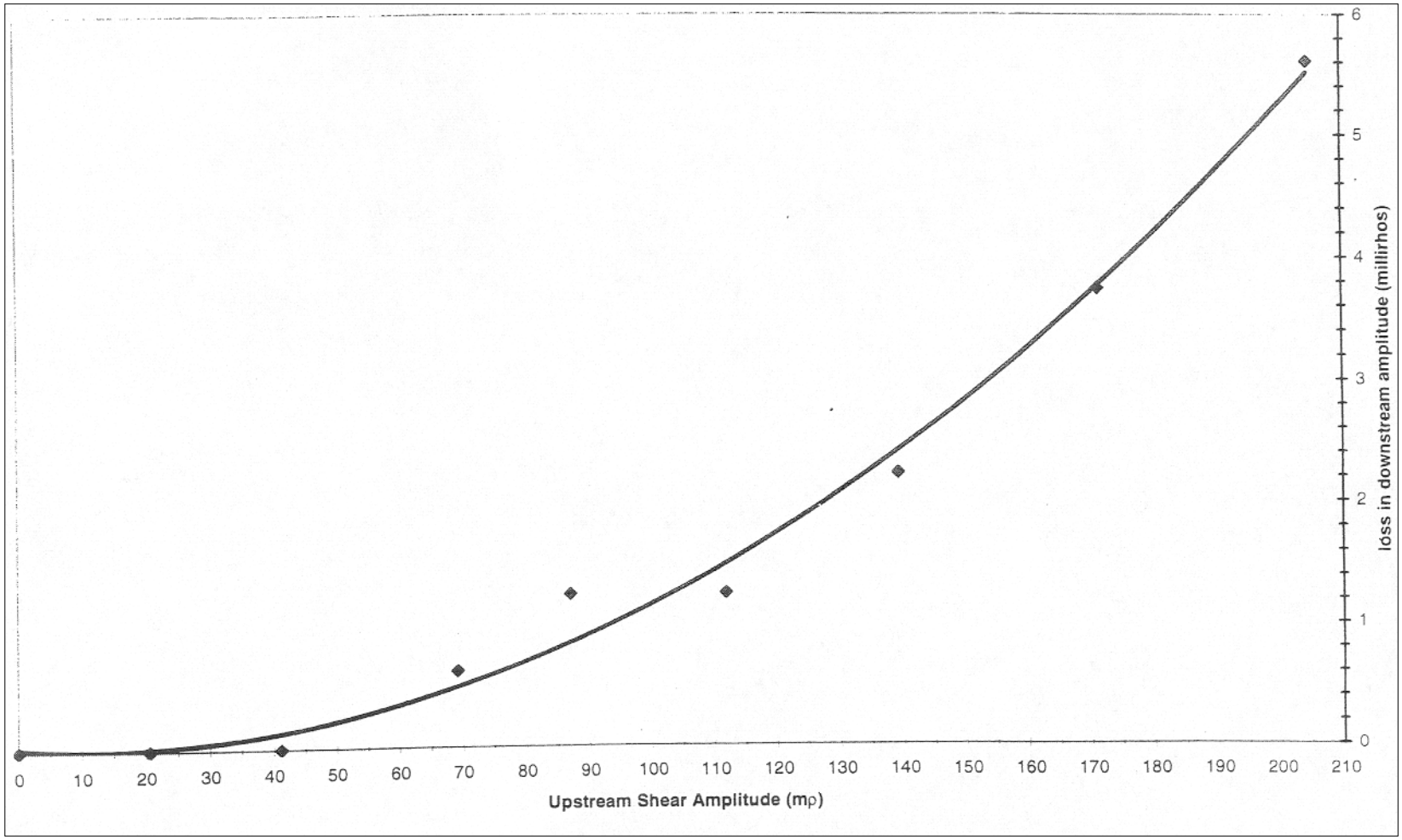

Figure 3-7
Percent loss in downstream crimp amplitude versus upstream shear amplitude

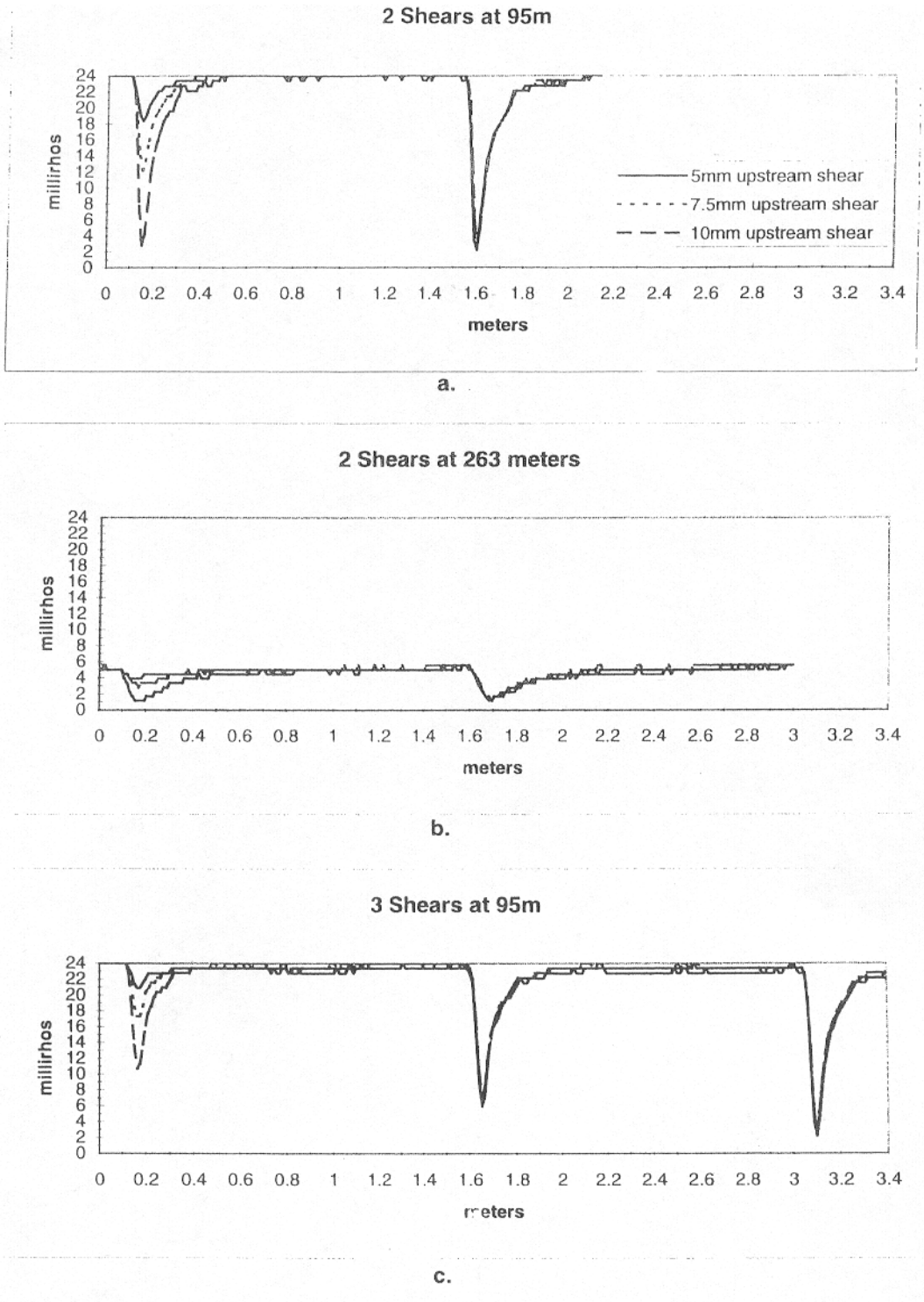

Figure 3-8: Effects of an increasing upstream shear reflection on a downstream 10mm shear reflection.

size. This difference results from the fact that after each shear was produced, the cable would elastically rebound slightly, decreasing the original size of the shear deformation and thus its corresponding reflection amplitude. However, regardless of amplitude size, the downstream shear reflections remained constant as the upstream shear deformation increased.

Thus far, it has been observed that the reflection width increases at a linear rate with distance, while reflection amplitude decreases with an exponential rate with distance. It was observed that the presence of a far upstream discontinuity led to a decrease in the downstream reflection amplitude. On the contrary, the interaction between two or three deformities at close separation distance but a great distance from the source was negligible, as long as the upstream reflections are less than 25 mρ or the shear displacement is not more than 50% of the cable diameter.

4. NUMERICAL APPROACH TO MODELING CABLE DEFORMATIONS

A finite difference model was chosen to model the wave propagation along the cable. Cable deformations affect the electrical properties of the cable such as capacitance, inductance and impedance. The numerical method equates a change in cable geometry at a specific location on the cable with a change in the electrical properties of the cable at that point. In this approach, electrical changes are accounted for as a lumped capacitance and resistance (Bilaine, 1994). As mentioned before, the inductance changes due to abrasion of the outer conductor of the cable are neglected. The geometry of a deformation is not directly considered in this model, only change in the capacitance associated with this deformation.

4.1. Mathematical approach of the problem

The model is based upon a frequency-domain finite difference solution of the transmission line equations (Taflove, 1996). Values of voltage, V, current, I, and frequency dependent resistance, R, are computed at each cell along the cable for each time step. By time stepping the equations, the incident pulse is tracked as it propagates along the cable. The number of time steps assigned to the model is dependent on the propagation velocity of the wave and the number of cells the wave will travel. The FORTRAN code is listed in Appendix A.

Frequency dependent loss is taken into account, through Fourier transform techniques to decompose time-domain signals into its various sinusoidal frequency components and an inverse Fourier transform routine. Once the signal has been subdivided into its various frequency components increasing loss coefficients may be applied to increasing frequency components. Once the higher frequency amplitudes have been proportionally reduced, the signal is recomposed into its time domain through an inverse transform.

The program allows the input of the nominal capacitance and inductance of the cable that need to be first calculated using cable characteristics such as inner and outer conductor diameters and relative dielectric permeability. Capacitive discontinuities can be introduced at any number of locations at any point, and their width can be spread over

one or several cells. The cell width may also be adjusted according to the size of the discontinuity to be modeled.

The transmission line equations for a wave propagating down a lossy coaxial cable are (Miner, 1996).

$$\frac{\partial V}{\partial t}(z,t) = -\frac{1}{C}\frac{\partial I}{\partial z}(z,t) - \frac{G}{C}V(z,t) \tag{4-1}$$

$$\frac{\partial I}{\partial t}(z,t) = -\frac{1}{L}\frac{\partial V}{\partial z}(z,t) - \frac{R}{L}I(z,t) \tag{4-2}$$

where: I = current, C = capacitance, V = voltage, R = resistance (frequency dependent), L = inductance (constant here), t = time. Equations (4-1) and (4-2) only account for frequency independent loss.

However, frequency dependent loss must be considered and thus added to the wave equations. To avoid numerical stability problems (Kath 1998), this loss is applied symmetrically. That is half to the voltage equation (4-1), half to the current equations (4-2). Let G* be the frequency dependent conductance added in parallel to the circuit and entering the voltage equation and R* the frequency dependent resistance added in series in the circuit and appearing in the current equation. To get stable solutions, G* and R* must be equal to one half of the total frequency dependent loss coefficient that we get from calibration as explained in section 4.7 called $loss_1$ (Kath, 1998).

The application of the loss in the code is done as follows. A first value of the current and voltage are computed taking only frequency independent loss into account using equations (4-8) and (4-9). Then, these voltages and current are transformed to the frequency domain using a Fourier Transform. The frequency dependent loss is applied to the Fourier Transformed voltage and current by multiplying them by the exponential as shown in equation (4-3).

$$R_k = e^{-\left(\sqrt{a_k}\right).A.\left(\frac{R_1}{2L}\right)dt} = e^{-\left(\sqrt{a_k}\right).A.(R^*)dt} \tag{4-3}$$

where: R_k is the frequency dependent loss at cell k, $R^* = \frac{R_1}{2L}$, R_1 is the frequency dependent loss coefficient or $loss_1$ from calibration as shown in Section 4.7 and L is the nominal inductance, A is the number of time steps between application of the frequency dependent loss and a_k is the component frequency on which R_k will be applied.

Equations (4-1) and (4-2) can be discretized into finite steps in time and space:

$$\frac{\Delta I}{\Delta z} = -C\frac{\Delta V}{\Delta t} - \frac{R}{2}V \tag{4-4}$$

$$\frac{\Delta V}{\Delta z} = -\frac{R}{2}I - L\frac{\Delta I}{\Delta t} \tag{4-5}$$

or:

$$\frac{I_{right} - I_{left}}{\Delta z} = -C\frac{V_{new} - V_{old}}{\Delta t} \tag{4-6}$$

$$\frac{V_{right} - V_{left}}{\Delta z} = -RI_{old} - L\frac{I_{new} - I_{old}}{\Delta t} \tag{4-7}$$

where: I_{right} = current at the next cell space during a particular time step, I_{left}: = current at the previous cell space during a particular time step, V_{right} = voltage at the next cell space during a particular time step, V_{left} = voltage at the previous cell space during a particular time step, I_{new} = current at the next time step to be calculated at a particular cell space, I_{old} = current at the previous time step to be calculated at a particular cell space, V_{new} = voltage at the next time step to be calculated at a particular cell space, V_{old} = voltage at the previous time step to be calculated at a particular cell space.

The FORTRAN finite-difference code computes the voltage and current at each cell by manipulating equations (4-5) and (4-6) into the following form:

$$V_{new} = V_{old} + \frac{1}{C}\frac{\Delta t}{\Delta z}(I_{left} - I_{right}) \tag{4-8}$$

$$I_{new} = \left(1 - \frac{R}{2}\frac{\Delta t}{L}\right)I_{old} + \frac{\Delta t}{L\Delta z}\left(\frac{V_{left} - V_{right}}{L\Delta z\left(1 + \frac{R\Delta t}{2L}\right)}\right) \tag{4-9}$$

At each time step, the voltage and current are first updated to account for the basic propagation in the waveguide using a centered finite-difference scheme through a leapfrog approach, (Kath, 1998). The 1-D wave equation can be written as follows.

$$u_t = u_x$$

Using central differences, one approximates any function, u, as:

$$\frac{u(x,t+dt)-u(x,t-dt)}{2dt} = \frac{u(x+dx,t)-u(x-dx,t)}{2dx}$$

Or:

$$u(x,t+dt) = u(x,t-dt) + \frac{dt}{dx}\left(u(x+dx,t)-u(x-dx,t)\right)$$

Starting with u(x,t-dt), one uses an approximate spatial derivative centered at (x,t) to get the value of u(x,t+dt). The picture is one of "leaping" from t-dt to t+dt. Then one goes from t to t+2dt, using the previously calculated values of u(x,t+dt) and so on and so forth. One advantage of the leap-frog method for modeling wave-propagation is that at precisely the (Courrant, Friedlich, Levy) CFL condition, that is when the time step equals the time the wave needs to cross one cell, the method is a discrete version of the wave equation and any input shape propagates without distortion.

As described above, the frequency dependent loss for that time step is then applied through an operator splitting technique (Kath, 1998). Resistance, R in equations (4-3) is split and the frequency dependent, R_1, and independent, R_0, parts of the loss are applied separately. The frequency independent part of the loss is applied at each time step, when the frequency dependent part is applied every "A" time steps in order to save on computation time. The parts of the signal for the voltage and current not including the source are transformed into the frequency domain and the proper amount of loss is applied to each frequency component.

Since the frequency dependent loss is computed every A number of computational cycles, the R1 should be multiplied by A to impose the correct amount of loss upon the signal as shown in equation (4-3). This assumes that the amount of frequency dependent loss that occurs during the propagation of the wave through A computational cycles equals A times the frequency dependent loss that the wave

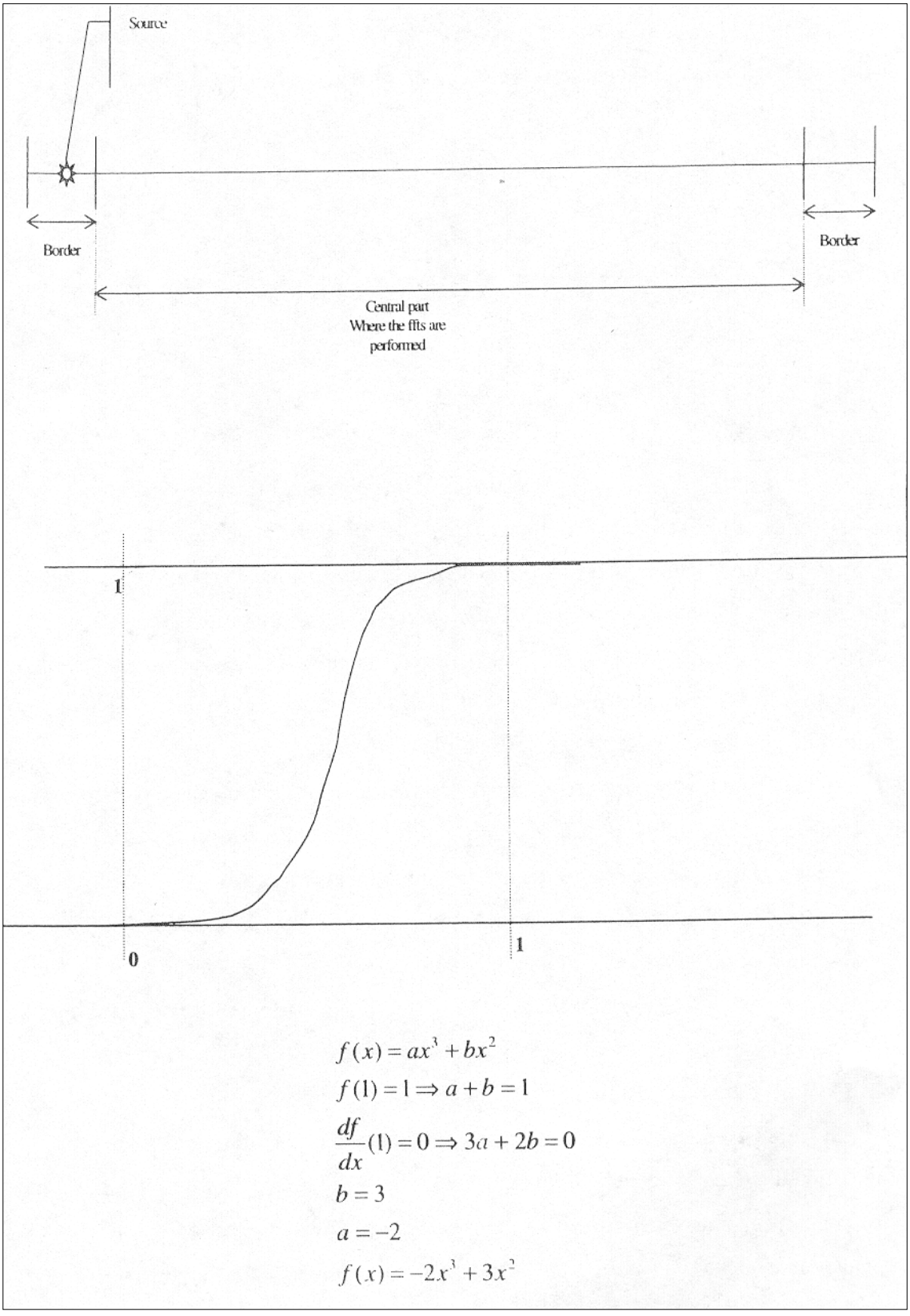

$$f(x) = ax^3 + bx^2$$

$$f(1) = 1 \Rightarrow a + b = 1$$

$$\frac{df}{dx}(1) = 0 \Rightarrow 3a + 2b = 0$$

$$b = 3$$

$$a = -2$$

$$f(x) = -2x^3 + 3x^2$$

Figure 4-1
Border geometry and smoothing polynomial function

undergoes during one cycle. At this time, the time step of computation is equal to the transit time across one cell. Therefore, the number of computational cycles, A, represents A cells. This assumption of linear increase in loss with each time step is only approximately true, and holds as long as A is kept relatively small with respect to the wave length of the higher significant frequency. The runs were performed with A=8.

The a_k power in equation (4-3) can be recast in terms of frequency. First consider that the length of the domain l_{fft} can be defined as the product of the cell width: $\Delta z = \frac{l}{n_{cells}}$ and the number of cells in the fft domain: n_{fft}.

$$a_k = \frac{2\pi(k-1)}{l_{fft}} = \frac{2\pi(k-1)}{\frac{n_{fft} l}{n_{cells}}}$$

since $l_{fft} = n_{fft}\Delta z = n_{fft}\frac{1}{n_{cells}}$

$$a_k = \frac{n_{cells}}{l}\frac{2\pi}{n_{fft}}(k-1) = \frac{1}{\Delta z}\frac{2\pi}{n_{fft}}(k-1)$$

The ratio $\frac{2\pi}{\Delta z}$ is the frequency increment Δf used to decompose the signal into its various frequency components. Thus as k increases, f increases by $\Delta f k$. Hence:

$$a_k = \frac{\Delta f}{n_{fft}}(k-1) \tag{4-11}$$

This derivation shows that the frequency dependent loss can be expressed as follows:

$$R_k = e^{-\left(A\sqrt{\frac{\Delta f}{n_{fft}}(k-1)}\right)\left(\frac{R_1}{2}\frac{1}{L}\right)dt} = e^{-A\frac{1}{\sqrt{n_{fft}}}\left(\frac{R_1}{2}\frac{1}{L}\right)\sqrt{\Delta f(k-1)}dt} \tag{4-12}$$

One can see in equation (4-12) that the frequency dependent loss is proportional to the square root of the frequency. However, another proportionality function other than the square root function could have been chosen.

The source interacts poorly with the Fourier transformation of signals at nearby cells, therefore, the edges of the domain near the source and terminus are located in a border, and the Fourier transform is applied only done on the central part of the domain.

In order to interpret model signatures, they must be transformed back into the physical, or time domain. However, transformation of transitory phenomena requires a zero value at the boundary. Thus, to be kept continuous, the response must be smoothed when linked to the boundaries. The boundaries of the domain are considered to be reflectionless.

4.2. Input to the code

The FORTRAN code reads the parameters in the input file whose format is shown in Appendix C. The numbers input in this file have units as shown below.

Cable length in meters
: Including the border region

Number of Fast Fourier Transform (fft) points
: Number of points over which the fft will be calculated. This is also he number of cells less the borders.

Number of border points
: Number of points on each side of the central zone on which the Fourier transform is calculated

Rise time (s)
: Time required to reach full voltage, as illustrated in Figure 4-2

Final time (s)
: Time at which the code should stop computing voltages

Loss rate 0 (dB/m)
: Frequency independent loss. Being very small, it was ignored for the runs performed herein

Loss rate 1 (dB/m)
: Frequency dependent loss that was calculated during the calibration process.

Nominal capacitance (Farads, F)
: Capacitance for cells where there is no crimp or shear.

Nominal inductance (Henrys, H)
: Inductance for cells where there is no crimp or shear. The model was operated without changes in inductance at shears or crimps.

Source location
: Number of cells separating the source from the beginning of the cable (left extremity of the cable). To avoid any numerical instability due to the interaction between the source and the Fourier Transform, this number should be smaller than the number of points in the borders.

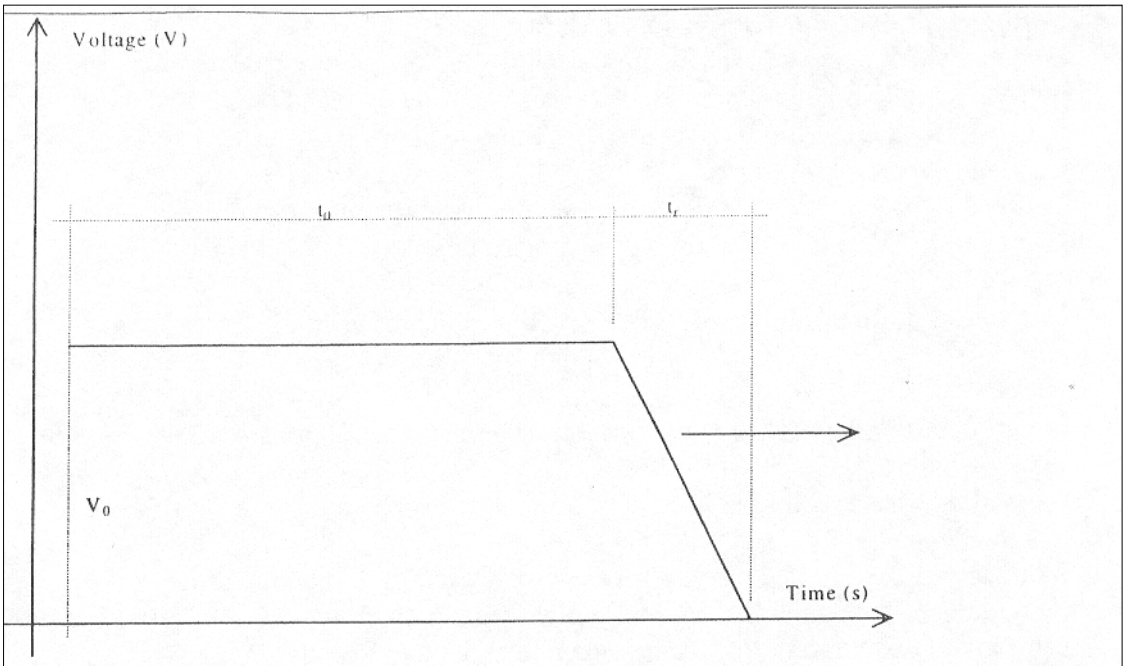

Figure 4-2a
Incident pulse

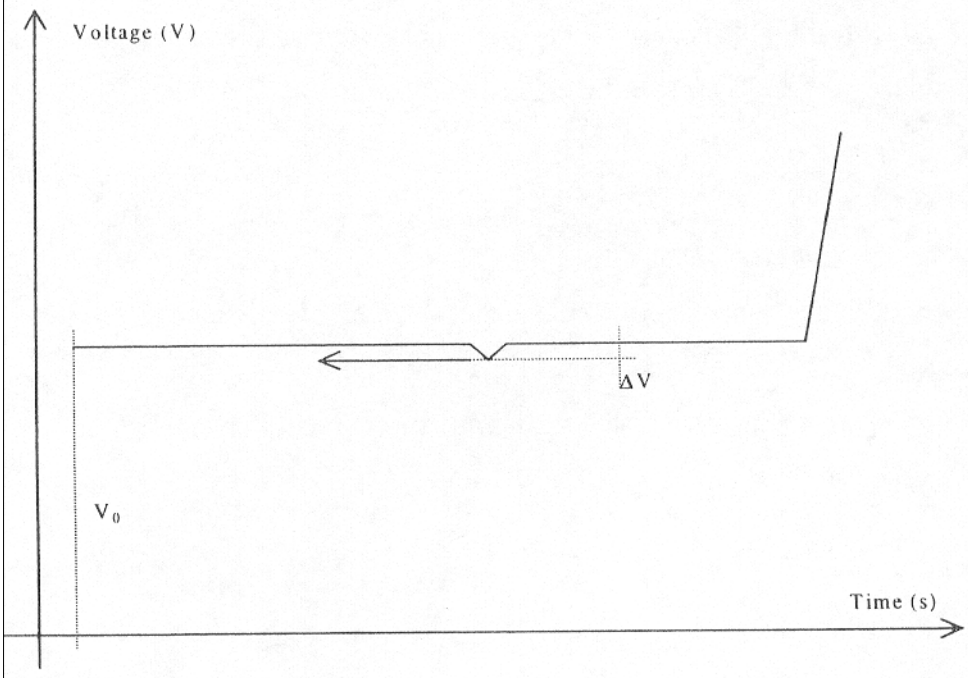

Figure 4-2b
Reflected pulses show spikes produced by changes in capacitance.

Figure 4-2: Shape of TDR voltage pulses. Initial pulses typically have short rise times, t_r, of 200 picoseconds, and long durations t_0.

Interval for calculating loss (number of time steps)

Frequency dependent loss calculation requires the computation of two ffts which imply a long computational time: therefore, the code allows the user to calculate this loss at a larger time interval than the time step.

Output interval (number of time steps)

To save on running time, it is also possible to write the output at a larger time interval than the time step: this is the output interval.

Number of crimps

Number of crimps you want to add along the cable. This should be an integer number

Crimp location

Location of the first crimp in number of cells (number of points from the source)

Capacitance at crimp

Capacitance at the crimp or shear location, which is larger than the normal value

Inductance at crimp

Inductance taken at the crimp or shear, in this work, it will be the same as the nominal inductance since inductive discontinuities are not taken into account. However, by inclusion in the formulation, inductance may be taken into account in other applications of this model.

The format of the numbers is important for proper operation. All integers must be input as integers and all real numbers must be input as real numbers. For example: do not write 2 for the frequency dependent loss but 2.0 and do not write 200.0 for the crimp location but 200.

4.3. Inductance and capacitance

Inductance, L, and capacitance, C, are dependent on the geometry and dielectric material of the cable. Capacitance and inductance for any non-deformed cable are calculated from the cable's geometry and electrical properties in the following fashion, per meter of cable (Taflove, 1996):

$$L = \frac{\mu_0}{2\pi} \ln\left(\frac{r_{outer}}{r_{inner}}\right) \tag{4-13}$$

$$C = 2\pi\varepsilon_0\varepsilon_{rel} \ln\left(\frac{r_{outer}}{r_{inner}}\right) \tag{4-14}$$

where: $\mu_0 =$ permeability of free space ($\mu_0 = 4\pi 10^{-7}$H/m), $\varepsilon_0 =$ permittivity of a vacuum ($\varepsilon_0 = 8.854.10^{-12}$F/m), $\varepsilon_r =$ relative permittivity of the dielectric material, $r_{inner} =$ inner conductor radius, $r_{outer} =$ outer conductor radius.

When the cable is sheared or crimped, its capacitance will change locally. This change is lumped into ΔC that represents the change in capacitance for one given cell. The lumped capacitance change per unit deformation must be measured for each cable as will be discussed in section (4.7).

4.4. Selection of a Cell Width

Figure 4-3 shows the cell analog of an elemental length of the transmission line. Each unit represents a finite difference cell of length Δz with variable values of capacitance, C, which represent changes in the cable geometry. The cell width should be chosen small enough to model known discontinuities while maintaining high resolution. Crimp deformations are made in 12mm increments. A cell width of 6mm was chosen and thus, each crimp deformation increment is represented by the same change in capacitance in two adjacent cells. The spacing is also small enough to allow for detection of small discontinuities (<50mρ in amplitude).

Even though shear deformations are concentrated over a width of 2mm, the geometry of the cable can be affected over a width as wide as 25mm (Pierce, 1997). Modeling the discontinuity over only a 2mm-wide cell could not provide a wide enough reflection compared to the field data. Increasing the capacitive discontinuity would not increase the width of the reflection but did increase its amplitude. Consequently, it was chosen to increase the width of the discontinuity itself rather than the value of the change in capacitance over a 2mm wide cell where a shear had been introduced. For example, a particular shear reflection measured in the field at 2m was 67mm in width and 41mp in amplitude. When a 2mm cell discontinuity was simulated in the model, its measured width was only 22mm. As the change in capacitance was increased in order to match the field reflection, the amplitude increased to values greater than 41mp, yet the width remained constant at 22mm.

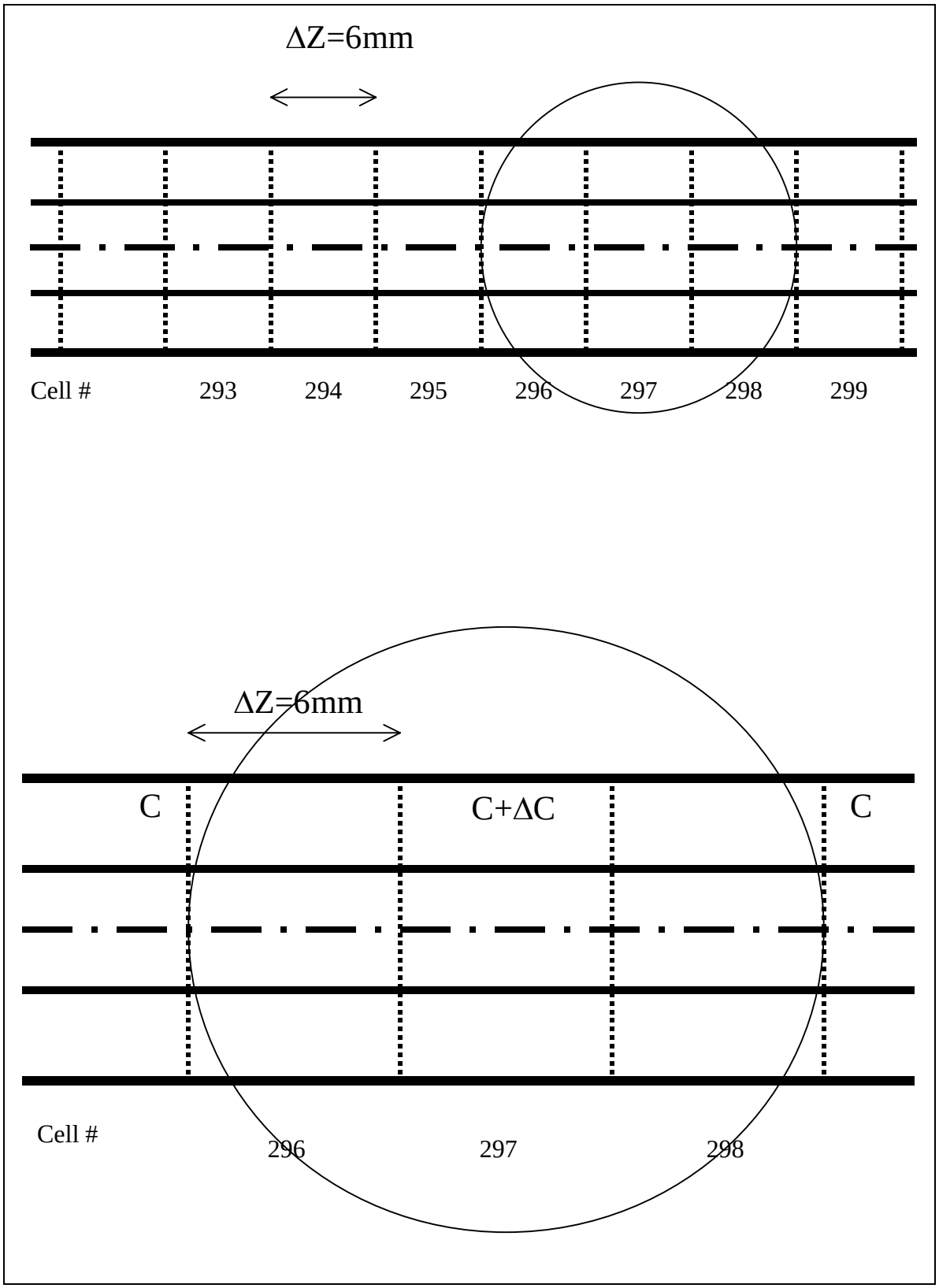

Figure 4-3
Cell model of the cable for finite difference calculations

Therefore, the only means available to increase the width of the reflection was to increase the width of the capacitive discontinuity. Additional experimentation revealed the reflection width matched the 2mm shear field data best when the width of the capacitive discontinuity approached 6mm. This approach is enforced by the fact that though the majority of the shear deformation will occur over the 2mm shear band, a significant amount of deformation occurs on both sides of the band (out of a total width of approximately 25mm).

Another approach would be to use a finer grid spacing and vary the values of the lumped capacitance over the area. Largest values would represent the 2mm shear band while significantly smaller values would represent deformations further away from the band. However, this approach is far more complex and requires more computation time for a limited increase in accuracy and was abandoned.

One can also reduce the cell width and see how the computed values evolve with the reduction of the cell width. This approach allows to select the smallest cell width for which computed values do not change when using a smaller cell width.

4.5. Incident pulse

The incident wave was based on the specifications of the cable tester, a Tektronix 1502B TDR pulser. As shown in Figure 4-4, the initial idealized pulse has a rise time of 200 picoseconds between the 10% and 90% points of the peak amplitude of one volt (Tektronix, 1975). Therefore, given a propagation velocity equal to the speed of light (c=$3.10^8 m.s^{-1}$), and a rise time, t_r, of 200 picoseconds in the modeled cable, the rising portion of the pulse will extend over a width,

$\Delta l = (200 \times 10^{-12} s)(3 \times 10^8 m \cdot s^{-1}) = 0.060m = 60mm$.

Since the model uses a 6mm cell width, the incident wave will extend over 10 cells.

As the cable is an imperfect conductor, the propagation velocity of the pulse will be less than the speed of light. For the cable used in the model, the propagation velocity, V_{prop} is $2.64 \times 10^8 m \cdot s^{-1}$. This velocity is calculated using the values of capacitance and

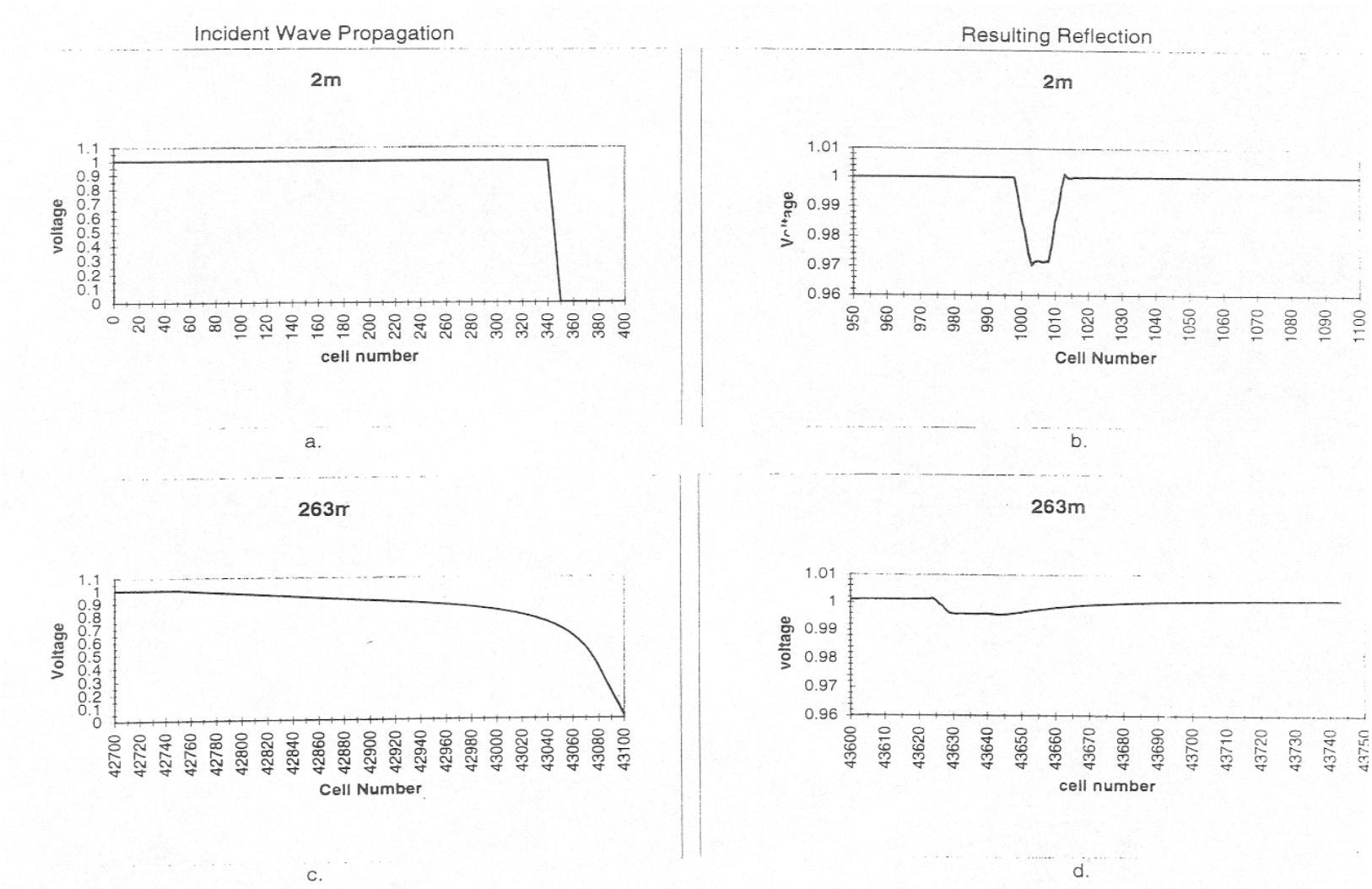

Figure 4-4
Comparison of the incident wave at 2m and 263m and its corresponding reflection signatures

inductance found in Equations (4-9) and (4-10) based on the cable geometry: (Taflove, 1996)

$$V_{prop} = \frac{1}{\sqrt{LC}} \tag{4-15}$$

Voltage and current of each cell is calculated every 2.27×10^{-11} seconds (cell width divided by the propagation velocity) which is the time necessary for the leading edge of the pulse to traverse one cell. The maximum time step between calculations is equal to the travel time. This time interval satisfies the Courant-Friderichs-Lewy (CFL) condition in the finite difference method, which requires the time step to be shorter or equal to the time necessary for the wave front to cross one cell. The time step used in the model is calculated as $\frac{\Delta z}{V_{prop}}$.

4.6. Resistance

Resistance needed to model any cable can be found by inspection of the shape of the incident wave (Taflove, 1996). As the incident pulse propagates down the cable, the rise time increases or the front spreads out in time or disperse, which affects the shape of any reflection discontinuity it encounters.

The value of the resistance assigned to Equation (4-3) is dependent upon frequency (Ramo, 1993), as losses caused by skin effect in a cable exhibit a frequency-dependant behavior. The reason why resistance is dependent upon frequency is that higher frequencies go over more cycles than smaller frequencies along the same propagation distance. Therefore, they undergo a larger amount of hysteric loss per unit length. Specifically, resistance is found to increase proportionally to the square root of the dominant frequency (Ramo 1993). However, other functions than the square root could be employed. The solution for the frequency dependent loss is made in the frequency domain.

A sharper slope in the signal indicates a higher frequency content (Taflove, 1997) and therefore will attenuate faster than a shallower slope because the high frequencies are the first to diminish. For example, a 4X rise time will require twice ($2 = 4^{1/2}$) as much distance to double than a rise time of X, due to high frequency attenuation along the

cable. Therefore, there is no need to recalibrate the model with changes the rise time since the model automatically accounts for changes in frequency. This is shown in Figure 4-5.

4.7. Resistance calibration

The first step in calibrating the model to the field data is to plot reflection width of known deformations versus transmission distance in Figure 4-6. Nine 12mm-wide crimps were placed at increasing distances along the cable and their reflection widths were measured using NUTSA (Huang, 1993). The second step is to measure the slope of the reflection width-distance relationship to determine the increase in reflection width over a specified distance. The slope was measured from zero to 100 meters. Based on this slope the reflection width is found to increase by 220% after traveling 100 meters. The value of the frequency dependent loss (loss $rate_1$) is adjusted to cause the reflected wave of the model to increase in width at the same rate as in the field data.

It is also important to consider what information the cable tester receives after launching a pulse through the cable. The signal on the screen shows the reflection magnitude and location on the cable. However, there is no information on the incident pulse or the effects of loss on the rise time. Therefore, the assumption was made that the rise time of the incident pulse in the model will increase at the same rate as the width of the reflected wave. Based on this assumption, the width and corresponding amplitude of the modeled reflection should be consistent with field reflections at increasing distances.

Calibration of the model can be accomplished in the following way. Assume it is desired to calibrate the model for a 50m cable. First approximate the loss coefficient by measuring the ratios of the reflection width created by a crimp located at 50m to that for a crimp located at 10m. Plotting a graph such that in Figure 4-7 might be helpful in this regard. Employ this value as the loss $rate_1$ for the loss coefficient and calibrate the change in capacitance necessary to produce a given reflection amplitude. Rerun the code for the same examples used to determine the first approximation and obtain a second value for the loss $rate_1$. It may be necessary to repeat the process several times until the required precision is reached. Given the uncertainties involved and the measurement errors, it is impossible to hope for more than a 10% precision on the calibrated parameters. Results

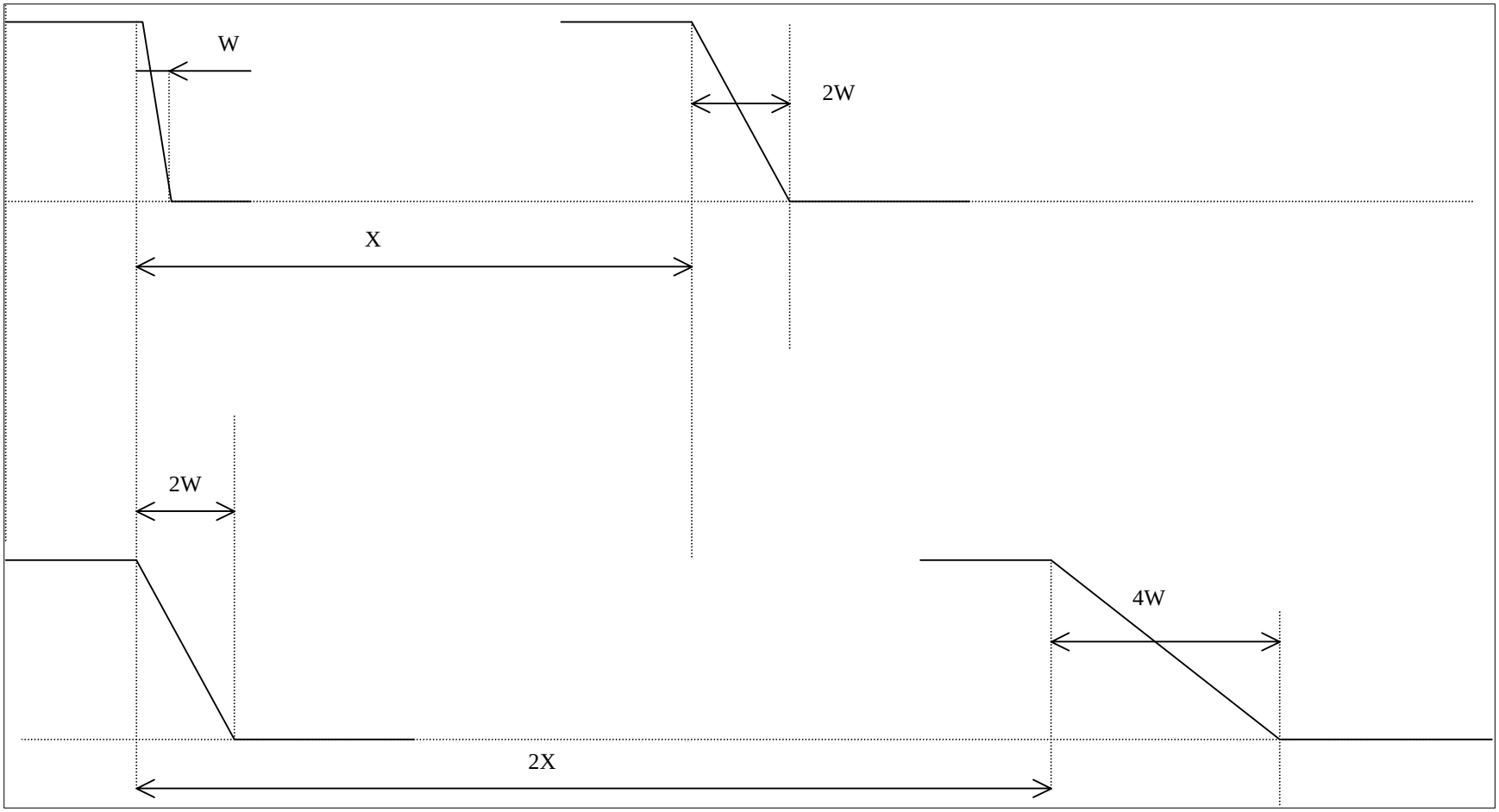

Figure 4-5
Effect of the increase of the rise time on the smearing of the wave front

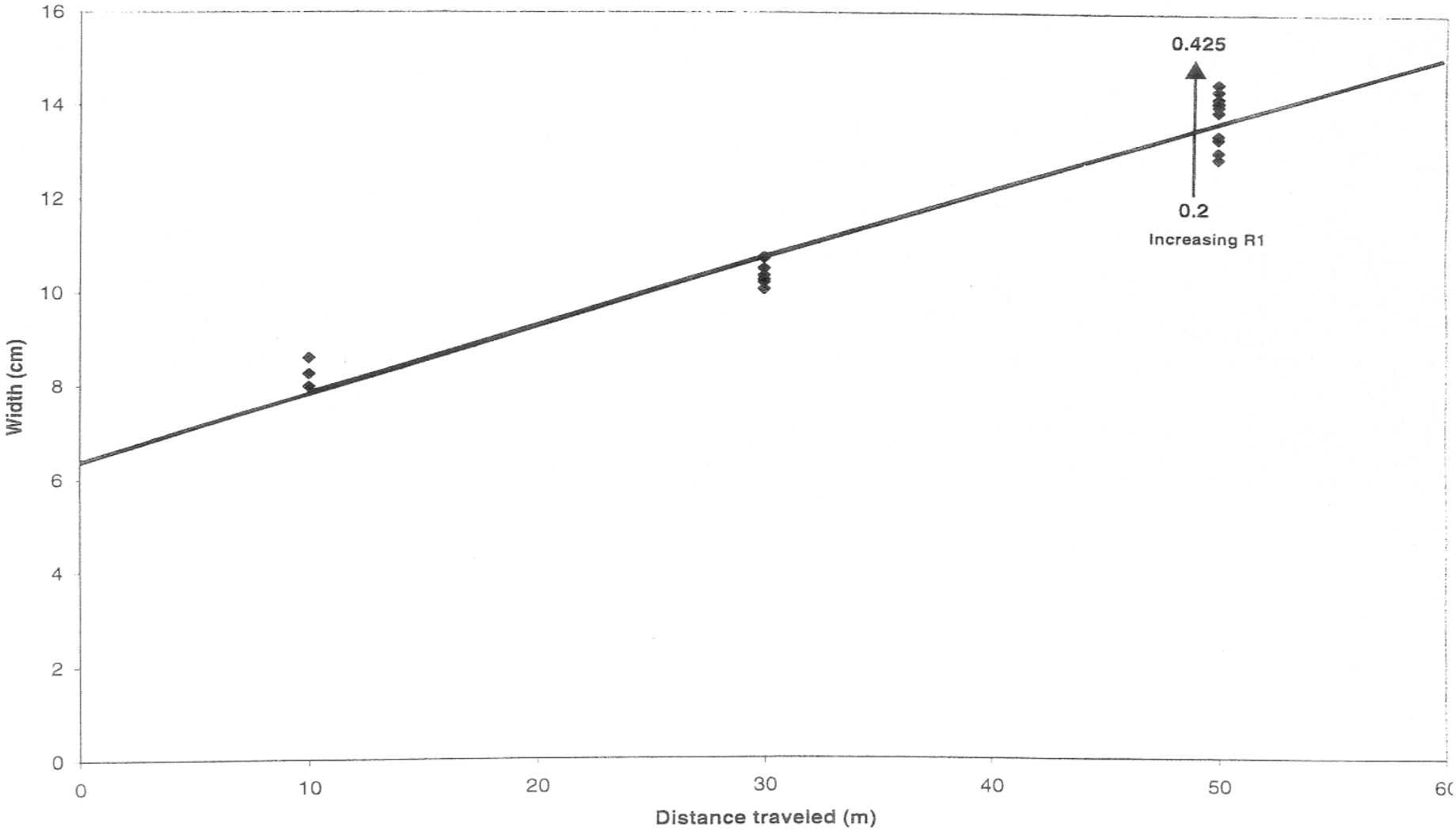

Figure 4-6
Width vs. distance travels for a standard 12mm crimp located at increasing distances from the source

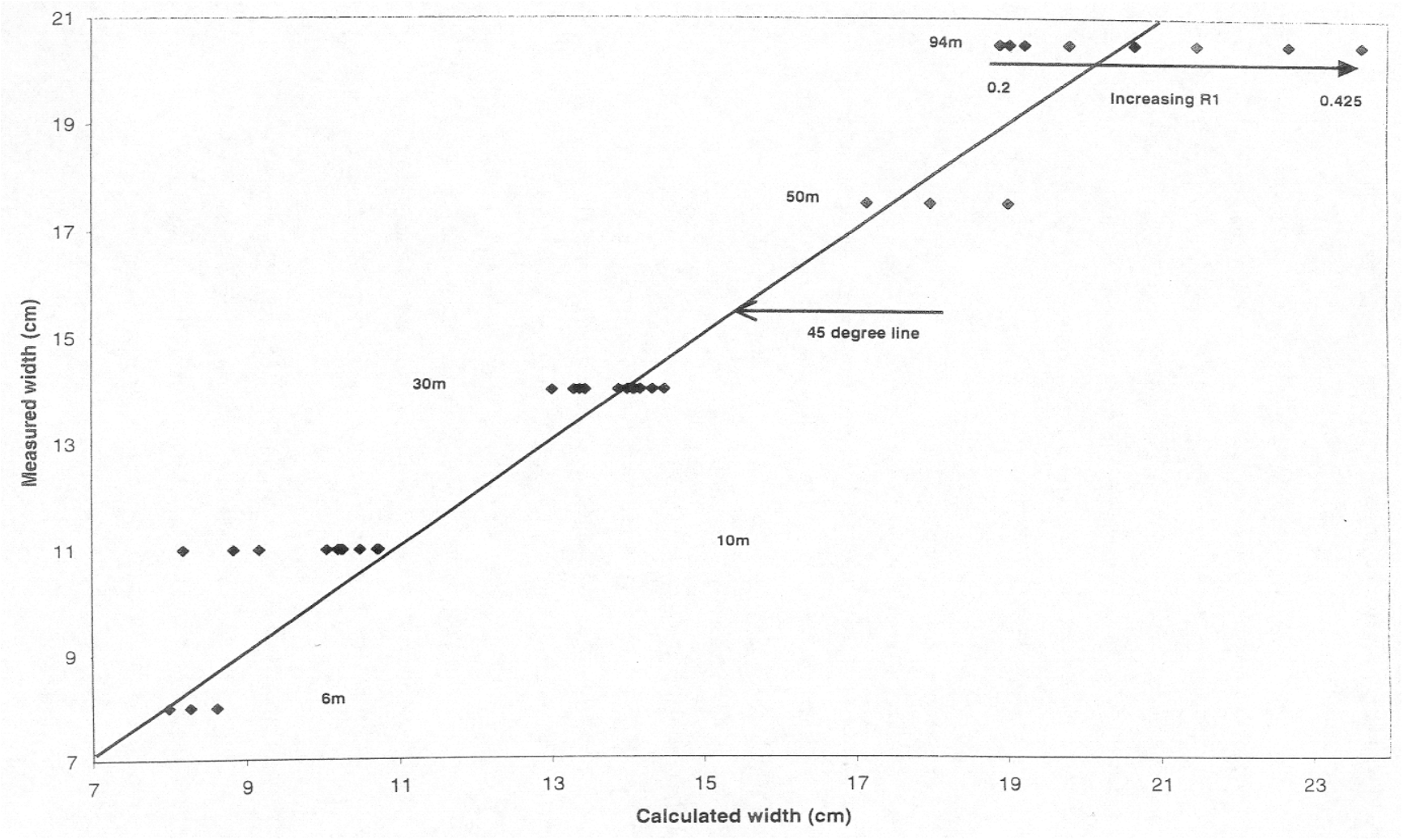

Figure 4-7
Measured vs. calculated widths for standard crimp located at an increasing distance from the source and different values of the frequency dependent loss coefficient

can then be replotted on a graph showing measured widths vs. calibrated widths to compare several loss rates.

It is important to be careful not to base the whole calibration on runs made for short propagation distances because those are far less accurate than for long propagation distances. For example, the sensitivity of modeled width to change in the loss rate at 10m is so low as to be non-existent. Only at 30m did the sensitivity increase, so as to be able to fit a loss rate to the width of a crimp-induced reflection. In addition the change in capacitance vs. cable deformation relationship is best determined from relationships developed at distances where deformities are expected.

4.8. Calibration of capacitive discontinuities

It is also necessary to calibrate a known shear and crimp deformation with an appropriate change in lumped capacitance. The capacitive discontinuity for a standard crimp was calibrated by matching the calculated amplitude of a modeled reflection to the measured amplitude of a reflection caused by a crimp of known dimensions. Since the model is to be used for propagation distances of about 50m, the capacitive discontinuity was calibrated at 50m. In this way, the modeled results match best the measured data for such propagation distances as 30m to 50m, which is the common length of TDR cables used in soils. The field crimp had a width of 12mm (2 cells) and a compressed diameter of 15mm (a standard 7.2mm crimp as described in Chapter 3) and was located at a distance of 51 meters. The resulting reflection amplitude for a crimped cable diameter of 15mm is 12mρ. The corresponding amplitude at 51m can be interpolated using the known measured amplitudes as being equal to 25mρ. The capacitive discontinuity was added to two 6mm cells. The change of capacitance necessary to create a 25mρ reflection at 50m is found by trial and error as being 120pF.

The same procedure was followed to calibrate the change of capacitance corresponding to a known shear deformation. A 7.5mm deep, 2mm wide shear displacement was located at a distance of 45m. A 22.5mρ amplitude was produced by the 7.5mm shear. The capacitive shear discontinuity was added to one 6mm cell. It was found by trial and error that a 150pF discontinuity is required to produce the 22.5mρ reflection amplitude at 45m.

Once the model is calibrated to capacitance changes at long distances, the same value of lumped capacitance can be used for shorter or greater distances to simulate the same discontinuity. Chapter 5 will compare modeled signatures and field data at larger propagation distances.

4.9. Additional assumptions and possibly interesting issues

There is an issue of when to observe the modeled reflection after it occurs. The model allows the propagation of the reflection back to the source. Since that is where the measurements are made in the field, these reflections were captured after their return, to be analyzed.

For relatively large loss rates such as 0.5dB/m and far from the source, the reflection spike may be sloped and the amplitude might become difficult to measure. For high loss rates such as these, a line is drawn tangent to the apex and the amplitude and width deduced from that tangent as shown in Figure 4-8.

The calibration procedure was developed independently of the limitation imposed by ignoring the return of the reflections. Furthermore, calibration of resistance is based upon the increase in measured width reflections produced by a single crimp at increasing distances.

Similar calibration of the lumped capacitance caused by a single discontinuity is calculated independently of travel distance. Thus, each calibration procedure is independent of either multiple discontinuity interaction or consideration of the return travel. Multiple deformations were studied in detail. Results of this study are presented in Chapter 5.

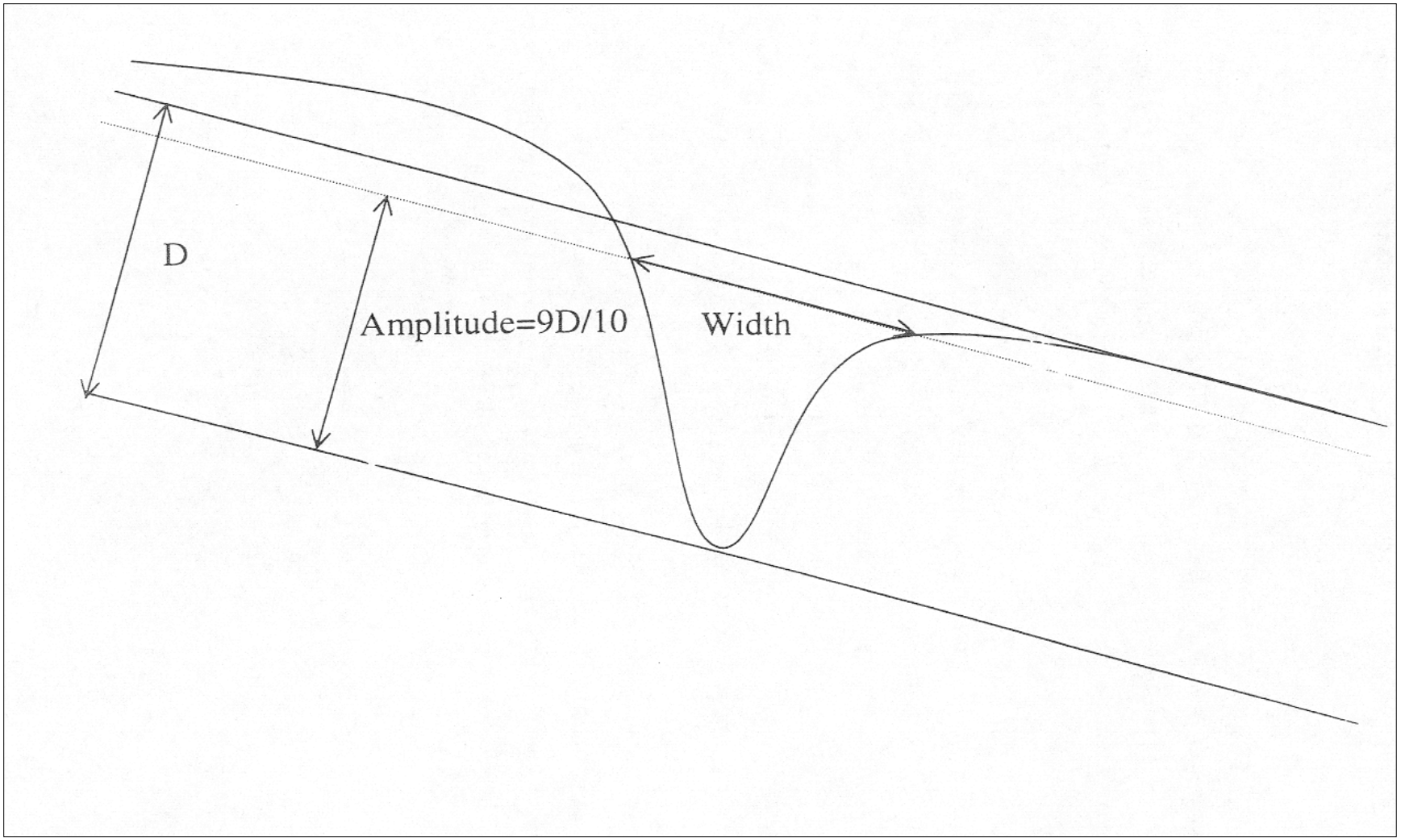

Figure 4-8
Measurement of the reflection widths for long travel distances of large amount of loss

5. COMPARISON OF SIMULATED AND MEASURED REFLECTIVE SIGNATURES

The goal of the model is to simulate reflections produced by known deformities in order to predict reflections produced by unmeasured interactive deformities. In order for the model to replicate this behavior, two calibrations are needed as explained in Chapter 4. First, frequency dependent resistance, R, must be calibrated by matching the increasing width of the incident pulse to the increasing width of standard crimp field reflections at increasing distances. Second, Capacitance, C, must be calibrated by matching modeled and measured crimp and shear amplitudes as these deformities increase in deformation with methods described herein. Calibration of C and R requires cable lengths of 20 m to 30m.

Once the frequency dependent resistance or loss and the capacitance sensitivity to cable deformation have been calibrated with field data, simulated reflections can be compared with measured reflections at longer distances. The use of frequency dependent loss allows accounting for all losses in the cable. Theoretically, it should not be necessary to calibrate a lumped capacitance to a reflection at longer distances since the lumped capacitance change is not function of distance. However, minor differences at 6m are greatly magnified at 100m. Therefore, the calibration should be made at the distances where the model is intended to be used.

5.1. Single Discontinuities

Reflection shapes measured in the field and produced by the model and compared in Figures 5-1 and 5-2. Figure 5-1 shows reflections caused by one 12mm crimp at 6m and 94m down the cable. Figure 5-2 compares reflections caused by one 7.5mm shear deformation at 45m and 92m down the cable. The widths and amplitudes of the reflections were measured with the methods outlined in Chapter 2. They are very similar to field measurements where spike-like reflections at small distances gradually become rounded with increasing travel distances.

However, computed shear reflections are symmetrical when measured reflections are not. This measured asymmetry may be due to the presence of an additional

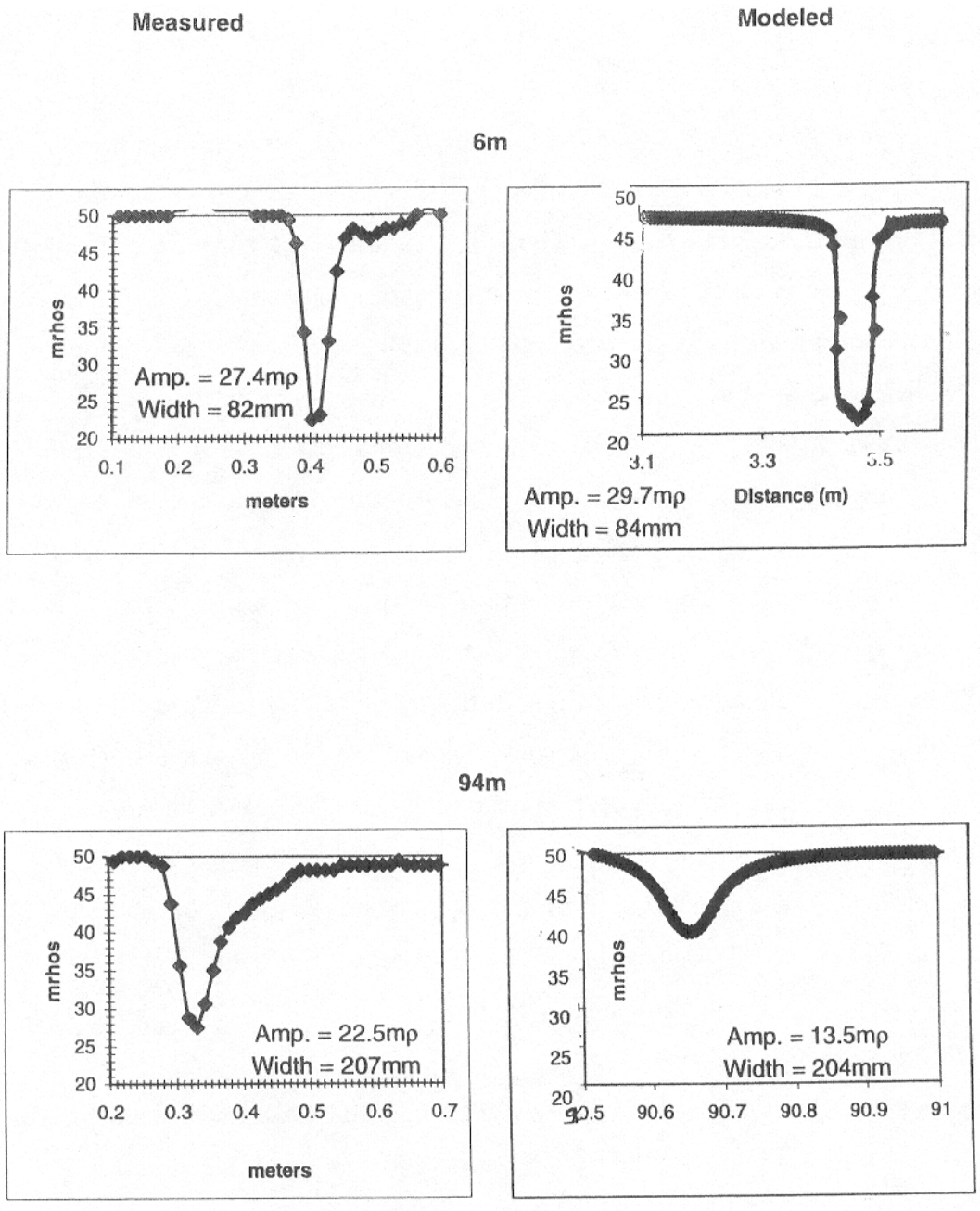

Figure 5-1: Comparison of measured and modeled standard crimp at 6m and 94m.

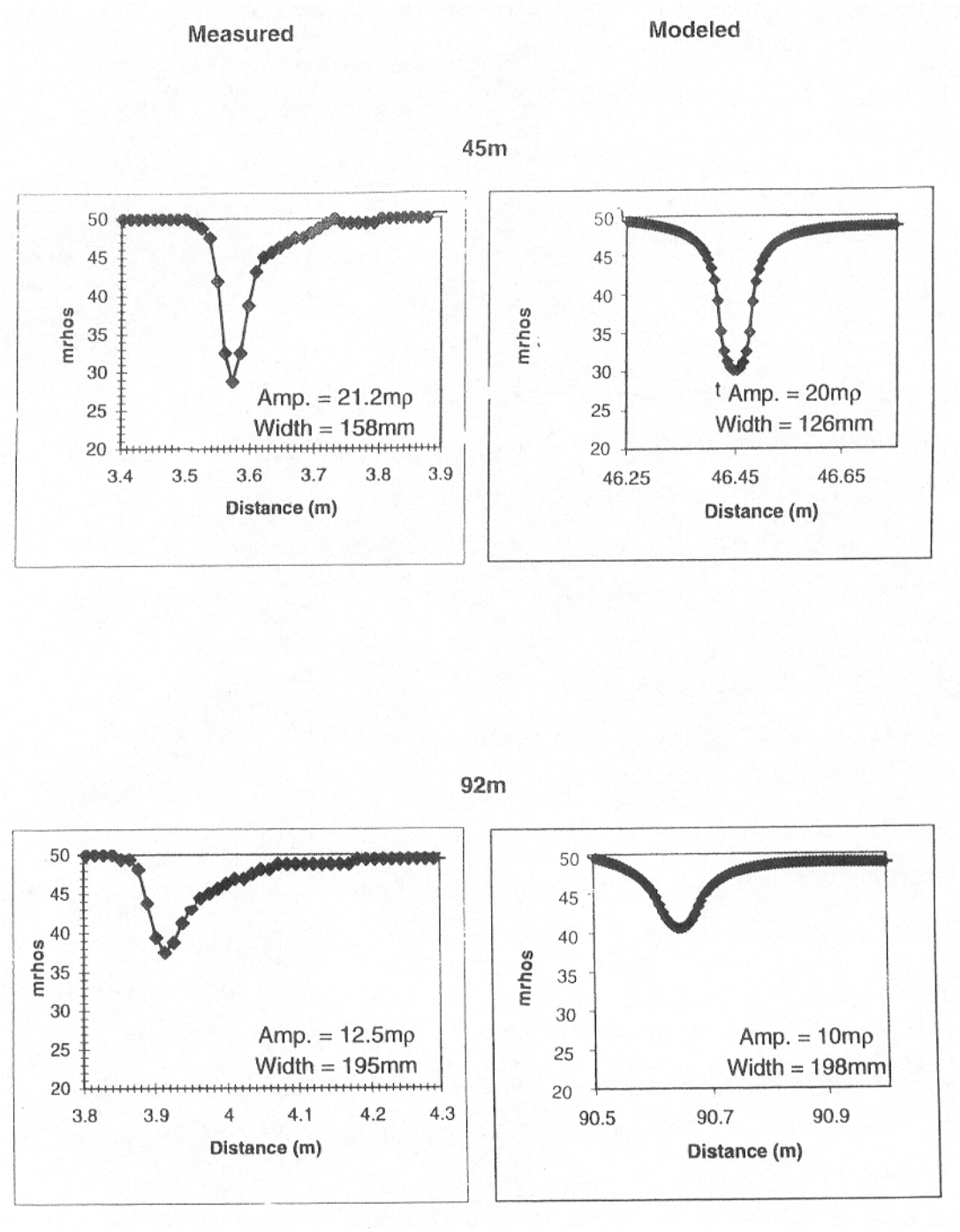

Figure 5-2: Comparison of measured and modeled 7.5mm shear displacement at 45m and 92m.

capacitance change in the wiring between the pulser and the beginning of the cable. Asymmetry could be produced in the model by choosing a smaller cell width, so that a shear is wider than one cell and smearing the capacitive discontinuity non-uniformly over these cells.

For the crimp located at 94m, the calculated amplitude does not match the measured amplitude very well. This disagreement is due to the fact that the calibration of the capacitive discontinuities was made so that the model replicates best the measured data between 30m and 50m. Such a difference with the present model can be avoided by calibrating the capacitance change for long travel distances such as 94m.

The initial slope of the reflection is steeper in the model than in the measured data. Once again, this is proportional to the rise time used in the model.

To compare the modeled results to the measured data more quantitatively, reflection widths are plotted versus propagation distance in Figure 5-3. Figure 5-4 shows the measured and calculated amplitudes and widths for crimps and shears as travel distance increases. The results show the model matching the signal geometry for both widths and amplitudes, in particular in the 30m to 50m region.

For shears, both for amplitudes and widths, the model matches best between distances of 30m and 50m where the model is intended to be used. The model for shears is more accurate for amplitudes than for widths at long propagation distances. For crimps, the calculated amplitudes do not closely match the measured results for propagation distances close to 94m either.

For both crimps and shears, the calculated results diverge from the measured at longer propagation distances. This is due to the fact that the resistance and capacitive discontinuity calibrations were made to best fit the measured and modeled data in the region ranging from 30m to 50m.

As mentioned in Chapter 3, Pierce et al (1994) described an exponential decrease in amplitude versus distance. However, this exponential decrease is not verified by the results of the code over short distances of less than 100m. However, the linear increase in width with propagation distance is verified by the calculated values, both for crimps and for shears.

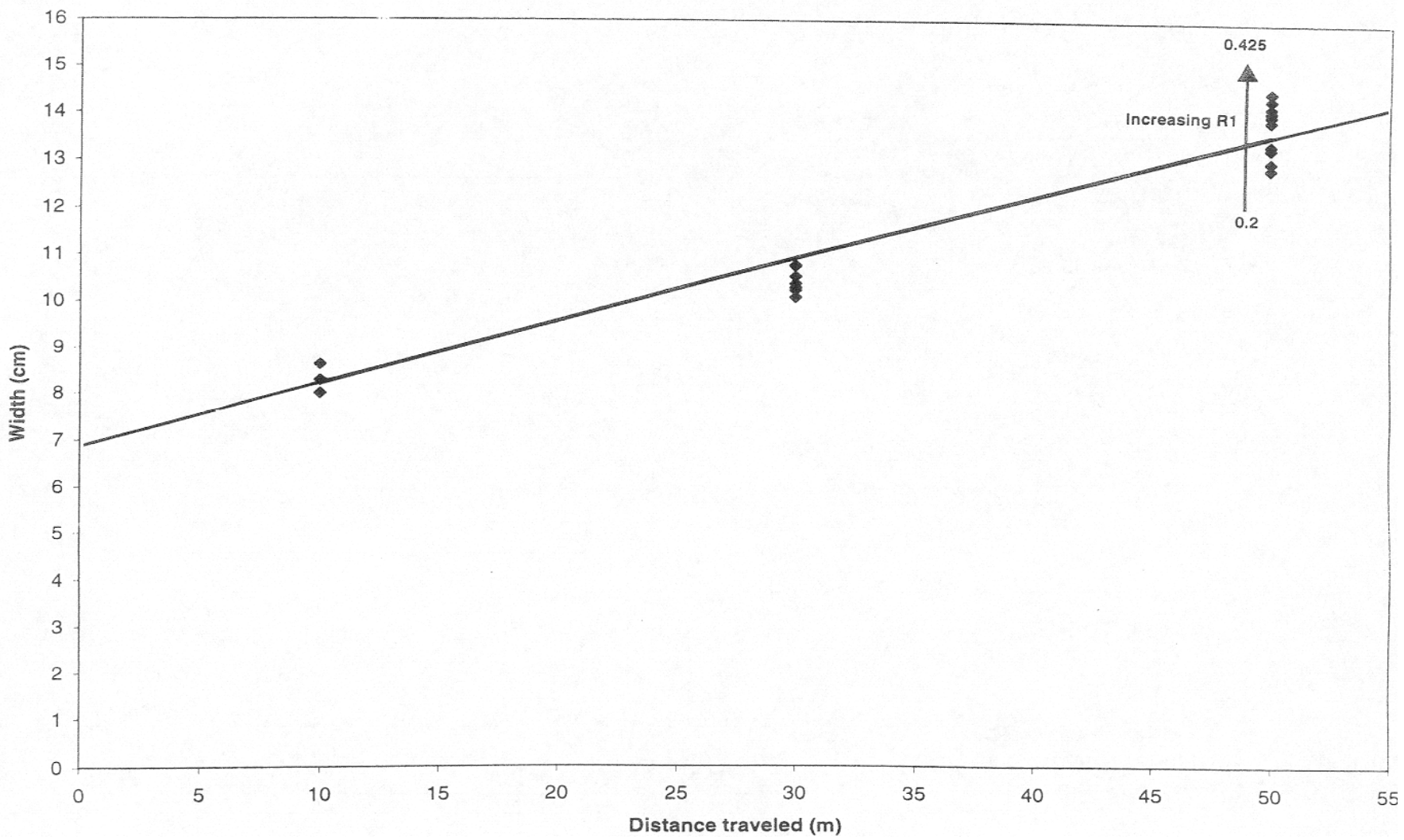

Figure 5-3

Width vs. Distance traveled for a standard 12mm crimp located at an increasing distances from the source

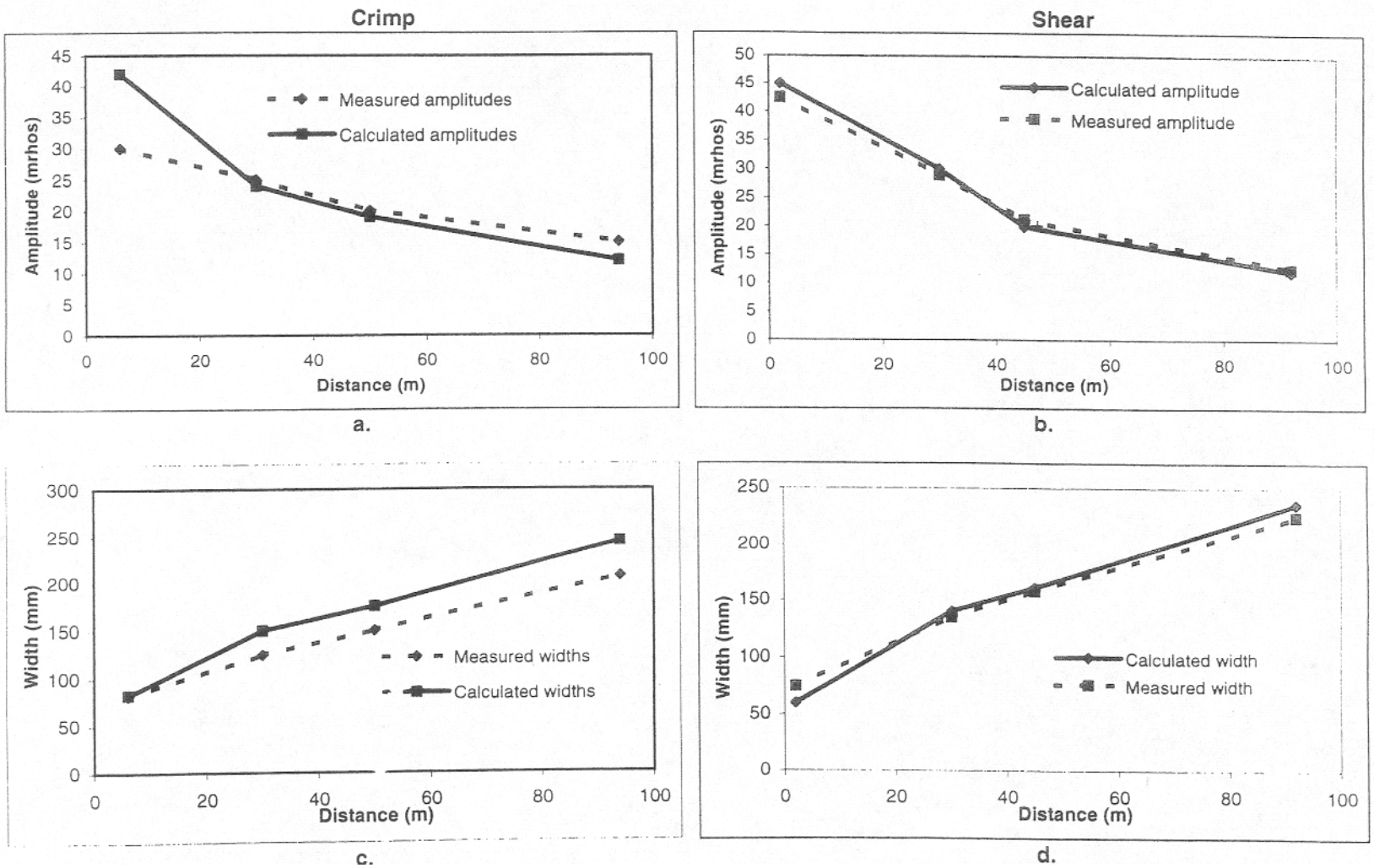

Figure 5-4: Comparison of measured and modeled reflection amplitude and reflection width vs. distance

Problems arise during data acquisition. Amplitudes are generally measured to an accuracy between 3 to 5mρ (Pierce, 1997). This accuracy is controlled by noise and other distortions that can vary the reflection amplitude by 5mρ. This inaccuracy becomes critical as amplitudes decrease with distance. As changes become smaller, noise and other distortions in the cable make it difficult to distinguish true reflections. Therefore, what is measured in the field is not necessarily the exact reflection for a given deformation.

5.2. Multiple discontinuities

As described in Chapter 3, field tests were performed to study the influence of a new reflection on downstream reflections. This interaction was modeled in a relative sense, because only a one-way path was employed. The comparative signals are only for a travel from the source through the upstream reflection off the deformity and then 5m back towards the source. Thus, the return path effects were not studied. However, using the results presented below, it is possible to predict the changes that these trends may undergo if the return path *was* studied.

5.2.1. Effect of an increasing shear at 2m on a downstream crimp at 51m

Increasing modeled shear reflection amplitude at 2m shows that the calculated reflections on a downstream crimp reflection at 51m have the same trend as those measured reflections. Figure 5-5 shows the calculated reflection signals. As the upstream shear deformity increases, the downstream crimp reflection amplitude slowly decreases and its width slightly increases. In addition the apex translates slightly towards the end of the cable. However, the model is less sensitive to upstream discontinuities than the field data measurement show, indeed, the model yields a 17% decrease in amplitude when the upstream shear is changed from a standard, 7.5mm deep shear to a 15mm deep shear, when the field data yield a 40% decrease in amplitude. The relative increase in width in both cases being very similar. If the return path had been modeled, the amplitude would have decreased by a larger amount than without considering the complete return of the reflection. However, the relative change in amplitude would have remained the same. Therefore, the results presented above are a good estimate of the sensitivity of the model to multiple discontinuities.

5.2.2. Effect of an increasing upstream shear at close proximity to another

The experiment performed by Pierce et al (1994) to study the interaction of multiple shears within close proximity to each other was also simulated. Two shears were modeled 1.5m apart at distance of 50 meters. Figure 5-6 shows calculated reflections. The upstream and downstream deformities are simulated by capacitive discontinuities. Both

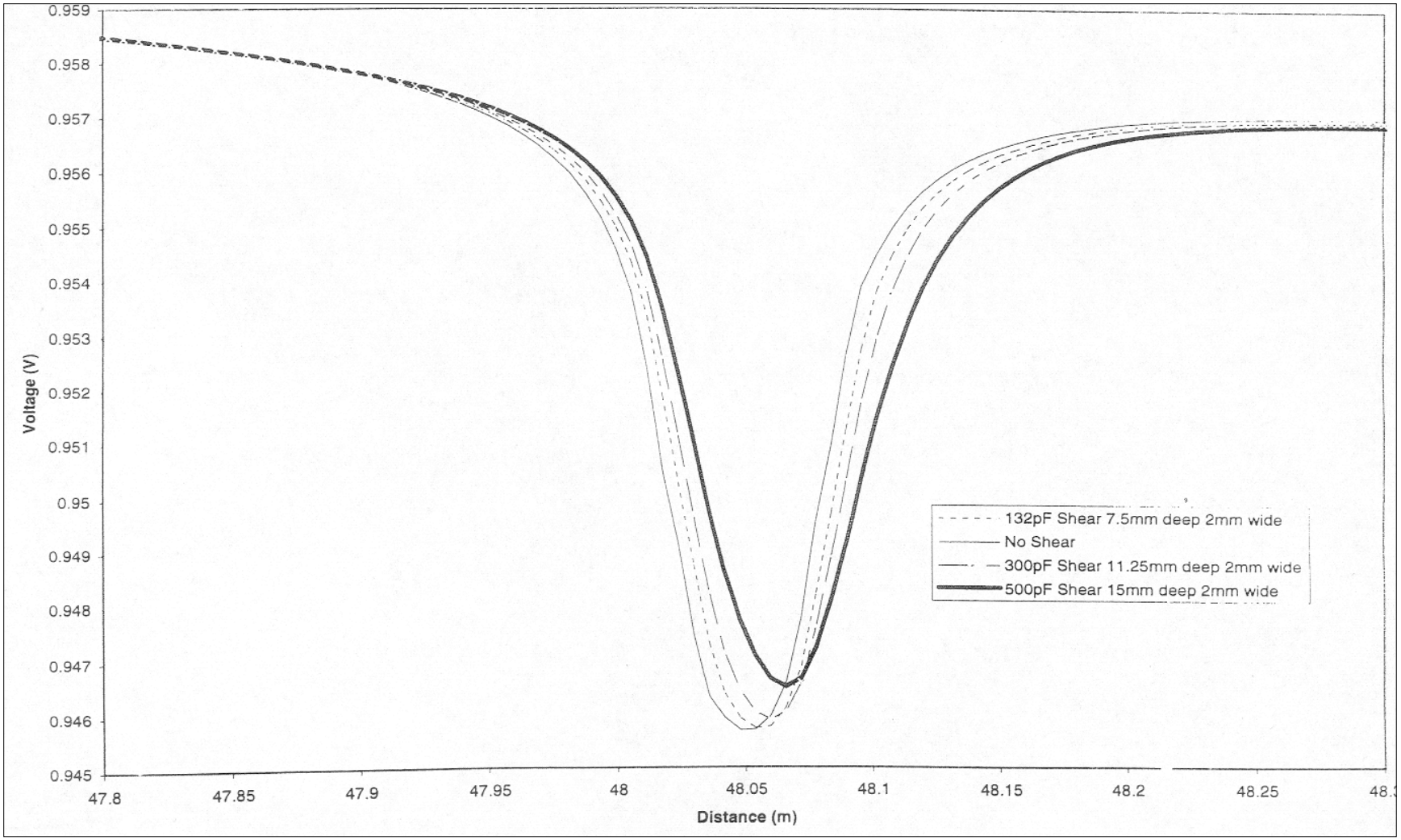

Figure 5-5
Effect of an increasing upstream shear deformation
at 2m on a downstream crimp reflection at 51m

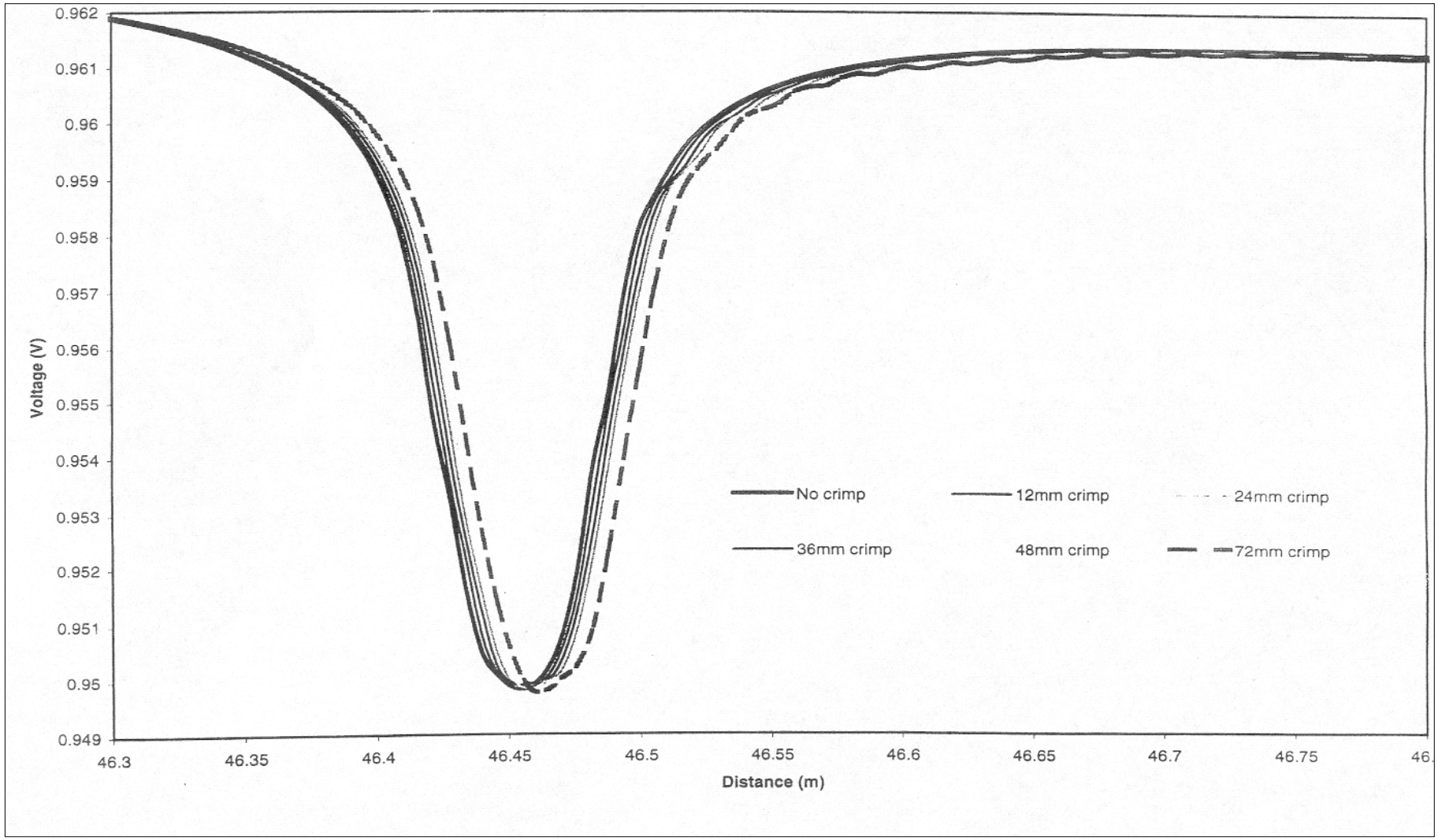

Figure 5-6
Effect of an increasing upstream crimp discontinuity on a downstream crimp at 51m

cases show a slight decrease in the downstream reflection amplitude and increase in width as the upstream reflection increases. For a 15mm deep shear located 1.5m upstream of a 7.5mm deep standard shear at 50m, the reflection amplitude decreases by 14% compared to the reflection caused by a unique standard shear at 50m. The measured data show essentially neither change in amplitude or in width for such interactions. This proves that the model is more sensitive to the interaction of a close upstream shear than the field data are.

As explained in the precedent paragraph, if the signal had been looked at after its return back to the source, the relative change in amplitude and width would have remained the same.

5.2.3. Effect of an increasing upstream crimp on a downstream crimp reflection

The effect of an increasing upstream crimp on a downstream crimp reflection was also examined. The results show almost no change in width or amplitude, which is consistent with the field data and the apex of the reflection on the downstream crimp translates also towards the end of the cable. Results are shown in Figure 5-7.

Considering the return path would again have led to the same trend, as was the case for the two precedent cases.

The results presented above show the same trends than the measured data. However, it is possible to have the amplitudes and widths match more closely by decreasing the frequency dependent loss coefficient ($loss_1$). The effect of the change in this coefficient on the widths and amplitudes of the reflected signal on a crimp at 50m is shown in Figure 5-8. These comparisons should be restudied by modeling the full return path to verify fully the model capability. However, since the amplitudes increase with a linear rate with propagation distance, considering the return path will only scale the reflection signal down but keep the relative decrease in amplitude constant.

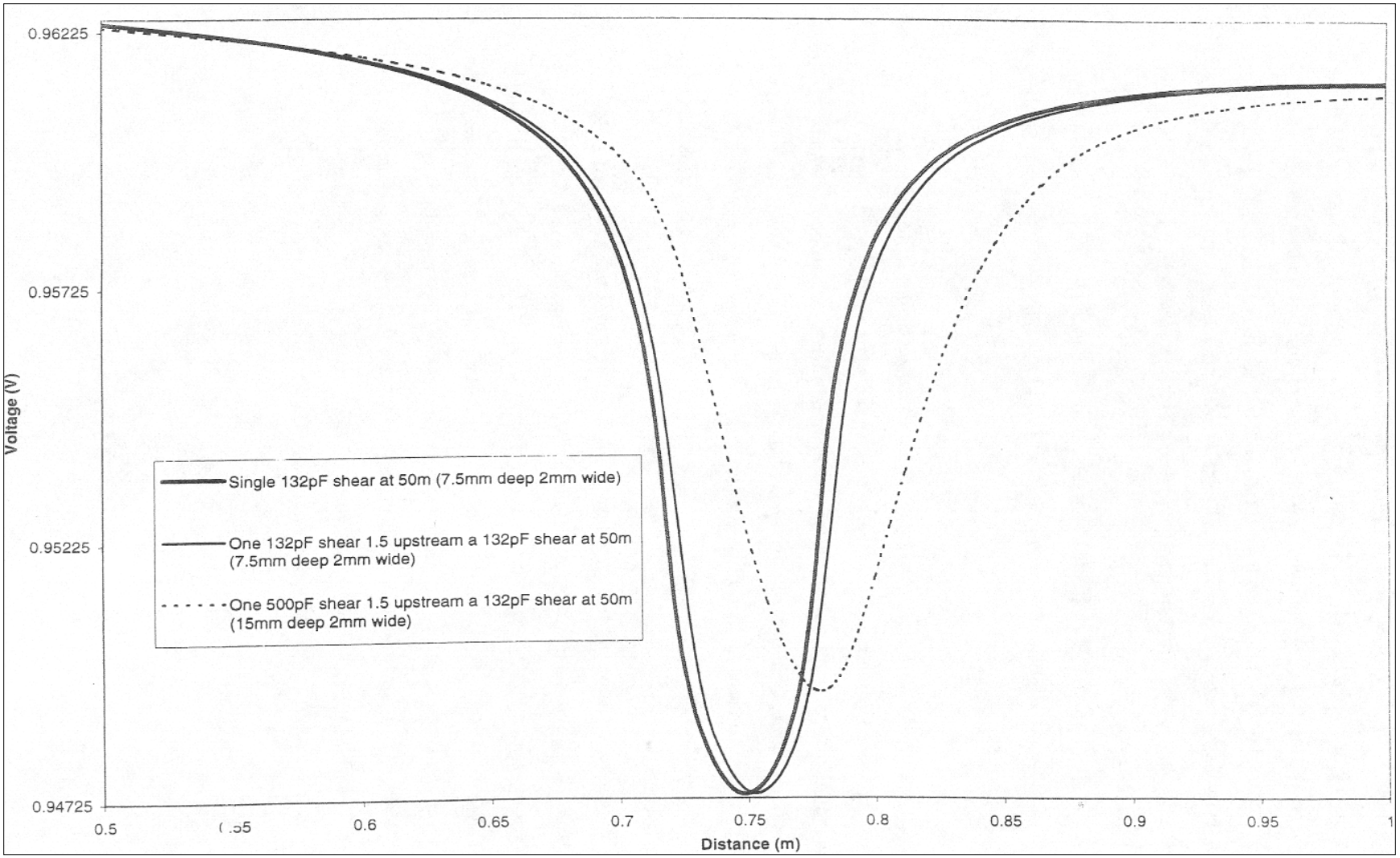

Figure 5-7
Multiple modeled shear discontinuities at close distance

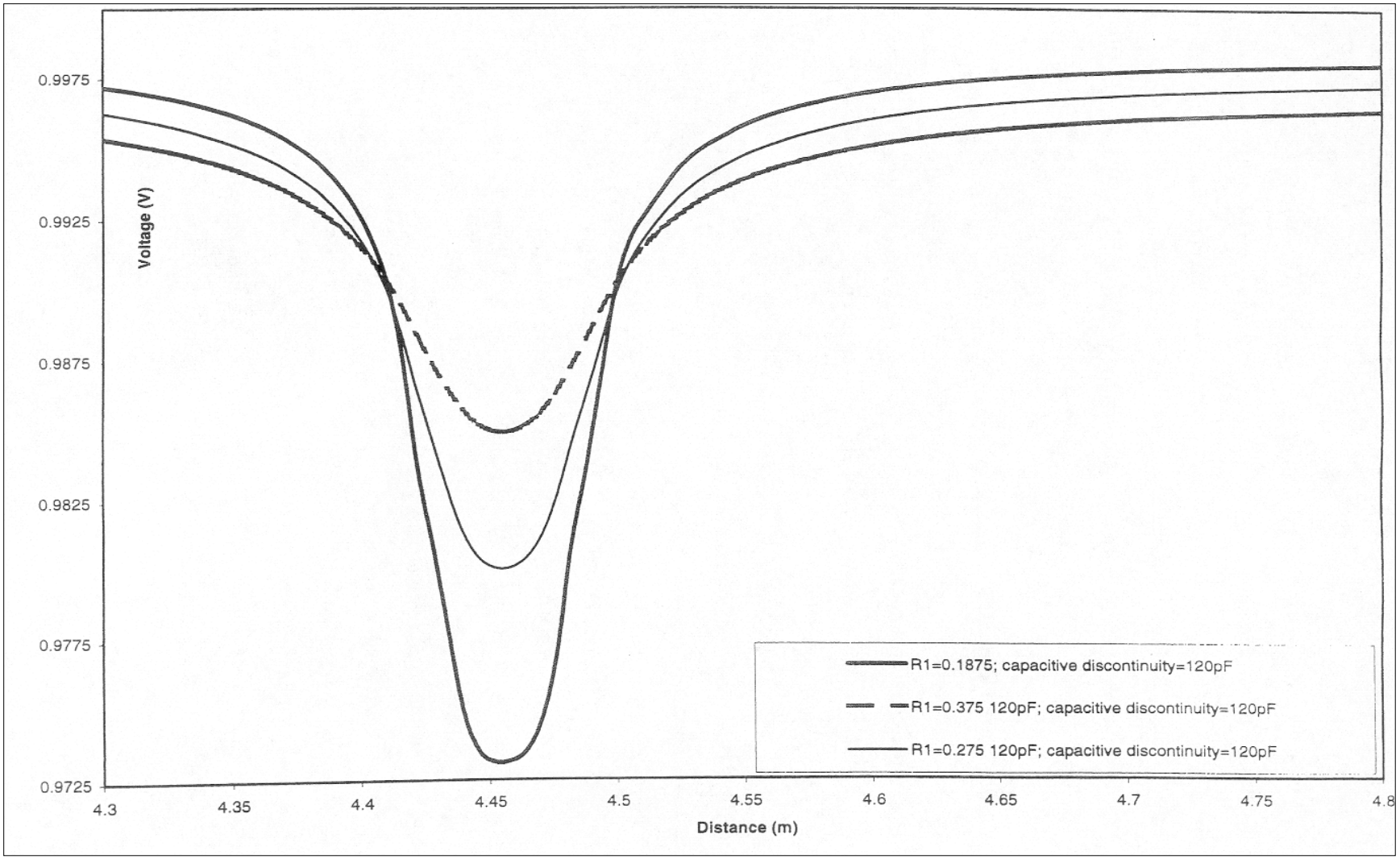

Figure 5-8
Effect of the change in the frequency dependent loss on the calculated reflections on a standard 12mm crimp located at 51m

6. CONCLUSIONS AND RECOMMANDATIONS

This thesis describes the ability of a Fourier Transform finite-difference model, based upon transmission line theory, to simulate the interaction between multiple cable discontinuities. The numerical simulation was calibrated for a specific metallic coaxial cable by producing controlled capacitive discontinuities by shearing and crimping the cable. Measured reflections were then compared to those calculated with the calibrated properties. Specifically, this approach successfully includes a frequency dependent resistive loss.

The following specific conclusions are tentatively drawn:

1. The frequency domain finite difference code proves to be a stable model for the partial differential equations that rule the one dimensional wave propagation in a waveguide. Symmetrical application of the loss to both current and voltage sufficiently suppresses instabilities.
2. Use of a Fourier Transform Technique to account for frequency dependent loss allows the calculated width of the reflected pulse to increase linearly with distance and the amplitude of the reflected pulse to decrease exponentially.
3. Calibration of the model requires two steps that involve the full length of cable to be employed. First, calibration of frequency dependent loss is accomplished by matching the measured and calculated linear increase in width of a reflection with increasing distance. Second, calibration of the reflection with a change in cable-geometry (or capacitance) is accomplished by matching measured and calculated changes in amplitude of the reflection with change in geometry.
4. At large propagation distances or for high loss rates, the steep slope of the front requires special consideration.
5. Multiple discontinuities were studied and the results showed that the model replicated the field behavior for multiple discontinuities located at small or large distances one from another. However, the comparison was only made for a “one-way” path, the return path was not studied and more work is needed to fully test the model.
6. Calculated signal reflections are symmetric rather than asymmetric as measured in the field. This difference requires more study.

7. Shear discontinuities were modeled with a single capacitive discontinuity spread over one six-millimeter cell. In reality, a shear deformity spreads over only two millimeters and is not uniform throughout. Future studies should investigate the effect of smaller cell sizes.
8. Inductive effects caused by irregularities in the outer conductor were neglected and should be investigated in future work.

REFERENCES

Bilaine, Christophe. Comparison of Numerical and Experimental Results to Evaluate Attenuation of Time Domain Reflectometry Waveforms Due to Multiple Discontinuities. M.S. Thesis, Northwestern University, Evanston, IL, 1994.

Dowding, C.H., and Huang, F.C. "Early Detection of Rock Movement with Time Domain Reflectometry". Journal of Geotechnical Engineering, ASCE, Vol., 120, No. 8, 1994.

Dowding, C.H., M. Su, K. O'Connor. "Principles of Time Domain Reflectometry Applied to Measurement of rock Mass Deformation". International Journal of Rock Mechanics, Mining Science & Geotechnical Abstracts, Vol. 25, No. 5, pp.287-297, 1998.

Huang, F.C., K. O'Connor, D. Yurchak, and C. Dowding. NUMMOD and NUTSA: Software for Interactive Acquisition of analysis of Time Domain Reflectometry Measurements. U.S. Bureau of Mines, Information Circular 9346, 1993.

Kath, W.L. (1998), Personal Communication. William Kath, Professor, Department of Engineering Science and Applied Mathematics, Northwestern University, Evanston, IL 60208.

Kroll, Christopher. Numerical Simulation of Measured Time Domain Reflectometry Signatures. M.S. Thesis, Northwestern University, Evanston, IL, 1997.

Miner, Gayle F., Lines and Electromagnetic Fields for Engineers. Oxford University Press, New York, 1996.

Pierce, Charles E., C. Bilaine, F. Huang, and C. Dowding. "Effects of Multiple Crimps and Cable Length on Reflection Signatures from Long Cables". Proceedings of the First Symposium and Workshop on Time Domain Reflectometry in Environmental, Infrastructure, and Mining Applications". Northwestern University, IL, 1994.

Ramo, Simon, J.R. Whinnery, and T. Van Duzer. Fields and Waves in Communication Electronics. John Wiley & Sons, Inc., New York, 1994.

Taflove, Allen. Computational Electrodynamics: The Finite-Difference Time Domain Method. Artech House, Boston, 1995.

Tektronix, Tektronix 1502 Cable Tester User's Manual. Beaverton, OR, 1975.

APPENDIX A

LISTING OF THE FORTRAN CODE

```
C..
      PROGRAM CABLE
      IMPLICIT DOUBLE PRECISION (A-H,O-Z)
      double precision ind,ind0,loss0,loss1,length,loss
      PARAMETER (nmax=32768)
      dimension ind(nmax),cap(nmax),volt(nmax),curr(nmax)
      complex*16 vtemp(nmax),vtempf(nmax)
      complex*16 ctemp(nmax),ctempf(nmax)
      dimension loss(nmax),z(nmax)
      CHARACTER*4    NUMSTR
      CHARACTER*9    FILENM
C
C     VARIABLES:
C
C     LENGTH = cable length (meters)
C     NFFT   = number of FFT points (region excluding border)
C     NBORD  = number of points in border
C     ISRC  = location or source point (grid point -- integer)
C     LMID  = loss calculation frequency (integer)
C     IMID  = plotting frequency (integer)
C     IMID  = plotting frequency (integer)
C     NSMOOTH  = number of points in smoothing region
C     CWIDTH = cell width (meters) = LENGTH/NFFT
C     NCRIMP = number of crimps
C     RISE   = rise time of source (seconds)
C     DT     = time step (seconds)
C     TF     = final time (seconds)
C     LOSS0  = loss coefficient, frequency independent part
C     LOSS1  = loss coefficient, frequency dependent part
C     CAP0   = nominal capacitance (Henries)
C     IND0   = nominal inductance (Farads)
C     CAP    = capacitance array
C     IND    = inductance array
C     CURR   = current array
C     VOLT   = voltage array
C

      OPEN (15,FILE='cable.in',STATUS='OLD')
      REWIND (15)
      READ (15,220) LENGTH
       READ (15,200) NFFT
      READ (15,200) NBORD
      READ (15,240) RISE
      READ (15,240) DT
      READ (15,240) TF
      READ (15,240) LOSS0
      READ (15,240) LOSS1
      READ (15,240) CAP0
      READ (15,240) IND0
      READ (15,200) ISRC
      READ (15,200) LMID
      READ (15,200) IMID
```

```
C
      CWIDTH = LENGTH/NFFT
      SPEED = 1/SQRT(IND0*CAP0)
      BORDER = NBORD*CWIDTH
      NCELLS = NFFT+2*NBORD
      ISMOOTH = NBORD
      fftwidth = length*nfft/ncells
      NTIME = TF/DT+0.5
       WRITE (6,*)
       WRITE (6,280) LENGTH, '... cable length'
       WRITE (6,260) NFFT, '... number of fft points'
       WRITE (6,280) CWIDTH, '... cell width'
       WRITE (6,260) NBORD, '... number of border points'
       WRITE (6,260) NCELLS, '... number of cells'
       WRITE (6,280) RISE, '... rise time'
       WRITE (6,280) DT, '... time step'
       WRITE (6,280) TF, '... stop time'
       WRITE (6,260) NTIME, '... number of time steps'
       WRITE (6,280) CAP0, '... nominal capacitance'
       WRITE (6,280) IND0, '... nominal inductance'
C
      pause

      DO 10 I=1,NCELLS
C        print *,i
        volt(i)=0
        curr(i)=0
        CAP(I)=CAP0
  IND(I)=IND0
  10  CONTINUE

      READ (15,200) NCRIMP
      DO 20 I=1,NCRIMP
        READ (15,200) JLOC
        READ (15,220) CAP(JLOC+NBORD)
        READ (15,220) IND(JLOC+NBORD)
  20  CONTINUE
      CLOSE(15)

 200  FORMAT (I10,14X,I6)
 220  FORMAT (F20.16,4X,I6)
 240  FORMAT (E20.16,4X,I6)
 260  FORMAT (8X,I10,12X,A40)
 280  FORMAT (8X,F20.16,2X,A40)

      pi=acos(-1.0)

c     store frequency dependent loss
call ffti(nfft)
      akmax=nfft*pi/fftwidth
      do 30 j=2,nfft/2+1
        ak=2*(j-1)*pi/fftwidth
        loss(j)=exp(-loss1*lmid*sqrt(ak)*dt/(2.0*ind0))
        loss(nfft-j+2)=loss(j)
  30  continue
      loss(1)=1.0

      do 35 j=1,nfft
```

```
       z(j)=1.0
  35   continue
       do 36 j=1,nbord+1
        x=dble(j-1)/nbord
        z(j)=3*x**2-2*x**3
        z(nfft-j+1)=z(j)
C       print *,z(j)
  36   continue

       VRIGHT=0.0
VLEFT=0.0
       cright=0.0

C
C main loop
C
       do 100 J=1,NTIME
       write (6,910) J
 910   format (1X,'cycle number...', I6)
c
c voltage source
c
       if ((J-1)*DT.LE.RISE) then
          f=(J-1)*DT/RISE
       else
          f=1.0
       endif
c
c update voltage
       print *,'... update voltage'
c
       do 50 k=2,ncells-1
        volt(k)=volt(k)-(dt/cwidth)*(curr(k)-curr(k-1))/cap(k)
  50   continue
       volt(1)=vleft
       vleft=volt(2)
       volt(ncells)=vright
       vright=volt(ncells-1)
       volt(isrc)=volt(isrc)+f
c

c update current
       print *,'... update current'
c
       do 60 k=1,ncells-1
        curr(k)=((1-loss0*dt/(2*ind(k)))*curr(k)
     & -(dt/cwidth)*(volt(k+1)-
volt(k))/ind(k))/(1+loss0*dt/(2*ind(k)))
  60   continue
       curr(ncells)=cright
       cright=curr(ncells-1)
if (mod(j,lmid).eq.0) then
        print *,'... do frequency dependent loss'
        do 70 k=1,nfft
          k2=k+nbord
          vtemp(k)=volt(k2)
          ctemp(k)=curr(k2)
  70    continue
```

```
        call fftf(vtemp,vtempf,nfft)
        call fftf(ctemp,ctempf,nfft)
        do 80 k=1,nfft
          vtempf(k)=vtempf(k)*loss(k)/nfft
          ctempf(k)=ctempf(k)*loss(k)/nfft
  80    continue
        call fftb(vtempf,vtemp,nfft)
        call fftb(ctempf,ctemp,nfft)
        do 96 k=1,nfft
          volt(k+nbord)=volt(k+nbord)*(1-z(k))+vtemp(k)*z(k)
          curr(k+nbord)=curr(k+nbord)*(1-z(k))+ctemp(k)*z(k)
  96    continue
       endif
c
c      add source to current
c
        curr(isrc-1)=curr(isrc-1)+f*sqrt(cap(isrc)/ind(isrc))
c
c      do output
c
        if (mod(j,imid).eq.0) then
        print *,'... do output'
          IK=INT(J/1000)
          IH=INT(J/100)-IK*10
          IT=INT(J/10)-IK*100-IH*10
          IO=J-IK*1000-IH*100-IT*10

NUMSTR=CHAR(IK+48)//CHAR(IH+48)//CHAR(IT+48)//CHAR(IO+48)
          FILENM='v'//NUMSTR//'.dat'

          OPEN (UNIT=12, FILE=FILENM)
          CLOSE (12, STATUS='DELETE')
          OPEN (UNIT=12, FILE=FILENM, STATUS='NEW')
          REWIND (12)
do 95 k=1,ncells
            write (12,900) (k-1)*cwidth,volt(k)
  95      continue
 900      format (1x,2f20.6)
          close(12)

        endif

 100    continue
        stop
        end

*
*****************************************************************
***
*
      subroutine fftf(fold,f,n)
      implicit none

c  fast fourier transform (forward) from numerical recipes
c  input array fold with real and imaginary parts in alternate
cells
c  upon return f contains its fourier transform
```

```
      integer nmax,div
      parameter (nmax=32768,div=2)

      integer n
      complex*16 fold(nmax),f(nmax)

      complex*16 x(nmax),z(nmax)
      common/cfft/x,z

      integer i,j,k
      integer ns,nq,nd,iq,id

      do k=1,n
         f(k)=fold(k)
      end do

      ns=1
      nq=n
do while (nq .gt. 1)
         nd=nq/div
         ns=ns*div
         iq=0
         id=0
         do i=1,ns
            do j=1,nd
               x(id+j)=f(iq+j)+conjg(z(id+1))*f(iq+j+nd)
            end do
            id=id+nd
            iq=iq+nq
            if (iq .ge. n) iq=iq-n
         end do

         if (nd .eq. 1) then
            do k=1,n
               f(k)=x(k)
            end do
            return
         endif
nq=nd
         nd=nq/div
         ns=ns*div
         iq=0
         id=0
         do i=1,ns
            do j=1,nd
               f(id+j)=x(iq+j)+conjg(z(id+1))*x(iq+j+nd)
            end do
            id=id+nd
            iq=iq+nq
            if (iq .ge. n) iq=iq-n
         end do
         nq=nd
      end do

      return
      end
c
```

```
c================================================================
=====*
c
      subroutine fftb(fold,f,n)
      implicit none

c  fast fourier transform (reverse) from numerical recipes
c  input array fold with real and imaginary parts in alternate
cells
c  upon return f contains its fourier transform

      integer nmax,div
      parameter (nmax=32768,div=2)

      integer n
      complex*16 fold(nmax),f(nmax)

      complex*16 x(nmax),z(nmax)
      common/cfft/x,z

      integer i,j,k
      integer ns,nq,nd,iq,id

do k=1,n
         f(k)=fold(k)
      end do

      ns=1
      nq=n

      do while (nq .gt. 1)
         nd=nq/div
         ns=ns*div
         iq=0
         id=0
         do i=1,ns
            do j=1,nd
               x(id+j)=f(iq+j)+z(id+1)*f(iq+j+nd)
            end do
            id=id+nd
            iq=iq+nq
            if (iq .ge. n) iq=iq-n
         end do
if (nd .eq. 1) then
            do k=1,n
               f(k)=x(k)
            end do
            return
         endif

         nq=nd
         nd=nq/div
         ns=ns*div
         iq=0
         id=0
         do i=1,ns
            do j=1,nd
               f(id+j)=x(iq+j)+z(id+1)*x(iq+j+nd)
```

```
            end do
            id=id+nd
            iq=iq+nq
            if (iq .ge. n) iq=iq-n
         end do
nq=nd
      end do

      return
      end
c
c=================================================================
=====*
c
      subroutine ffti(n)
      implicit none

c fast fourier transform initialization - from numerical recipes
c initializes sine and cosine vectors for fft routines

      integer nmax
      parameter (nmax=32768)

      integer n

      complex*16 x(nmax),z(nmax)
common/cfft/x,z

      integer j
      double precision dt,ang,pi,a,b

      pi=dacos(-1.d0)
      dt=(pi+pi)/dble(n)
      ang=dt

      z(1)=dcmplx(1.0d0,0.0d0)
      z(n/2+1)=dcmplx(-1.0d0,0.0d0)
      z(n/4+1)=dcmplx(0.0d0,1.0d0)
      z(3*n/4+1)=dcmplx(0.0d0,-1.0d0)

      do j=2,n/4
         a=dcos(((j-1)*2.0d0*pi)/dble(n))
         b=dsin(((j-1)*2.0d0*pi)/dble(n))
         z(j)=dcmplx(a,b)
         z(n/2-j+2)=dcmplx(-a,b)
         z(n/2+j)=dcmplx(-a,-b)
         z(n-j+2)=dcmplx(a,-b)
         ang=ang+dt
      end do

      return
      end
```

APPENDIX B

EXAMPLE RUN

The following input and output files correspond to the problem described below. It models the propagation of a 1V electric wave along a 98.304m long cable. A two cell, 110pF discontinuity is located at 50m from the left border.

Input file (cable.in)

```
98.304                      cable length(m)
16384                       number of fft points
40                          number of border points
0.000000000227311010        rise time (seconds)
0.0000000000227311          time step (seconds)
0.03724266372               final time
0.0                         loss rate 0 (per meter)
0.375                  loss rate 1 (per meter)
0.0000000000075767349124    nominal capacitance (in Farads)
0.000000189433594087        nominal inductance (in Henrys)
10                          source location
8                           interval for calculating fd loss
8150                        output interval
2                           number of discontinuities
8333                        location of discontinuity 1
11.0E-11                    value of discontinuity1 (in Farads)
0.000000189433594087        value of discontinuity1 (in Henrys)
8334                        location of discontinuity 2
11.0E-11                    value of discontinuity2 (in Farads)
0.000000189433594087        value of discontinuity2 (in Henrys)
```

Output file (v16300)

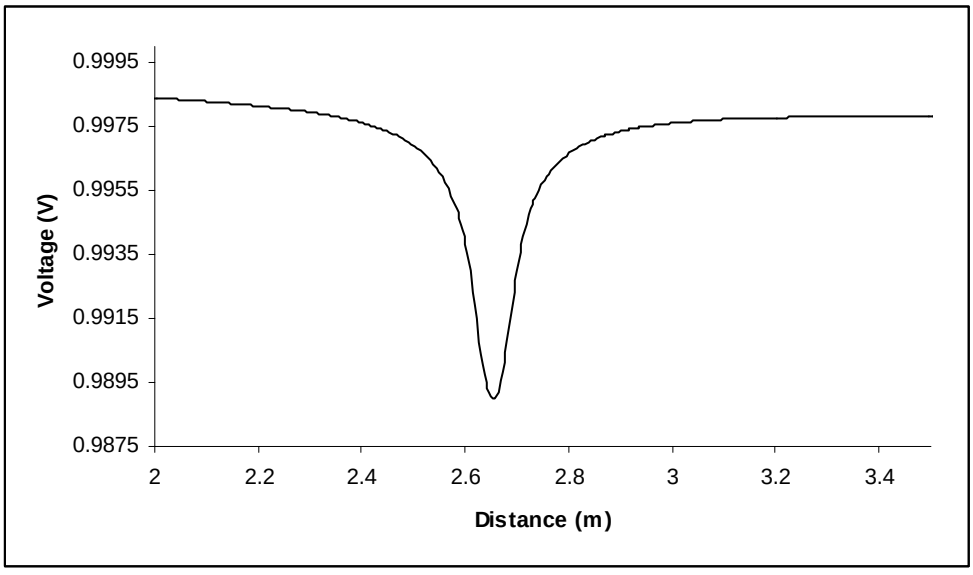

Sequence needed to be followed for data input

1. Choose the length of the cable: L
2. Choose the cell width: w
3. Compute N=Uw, which gives the number of w-wide cells to make up a L meters long cable.
4. Choose N' the number of fft points (cells) as the closest power of 2 larger than N.
5. Compute the new length of the cable corresponding to this new number of cells, N' given by L'=N'w.
6. Choose the number of border points, this choice is arbitrary.
7. Input the rise time corresponding to the pulser you are using.
8. Choose the time step, Δt, making sure that the CFL condition is satisfied, that is that the time step is smaller than the time needed for the wave to cross one cell, that is $\frac{1}{\sqrt{LC}}$, where L and C are the inductance and the capacitance of the cable.
9. Compute the final time: $t_f = \left(N' + 2 \cdot Borders\right) \cdot \Delta t$
10. Input the frequency independent loss rate corresponding to the cable used.
11. Input the frequency dependent loss rate. This parameter is given by the calibration procedure.
12. Input the nominal capacitance and inductance corresponding to the cable used. They are given by the following formulas, as explained in more detail in section 4.4.

$$L = \frac{\mu_0}{2\pi} \ln\left(\frac{r_{outer}}{r_{inner}}\right)$$

$$C = 2\pi\varepsilon_0\varepsilon_{rel} \ln\left(\frac{r_{outer}}{r_{inner}}\right)$$

13. Input the source location. The value input must be smaller than the number of border points.

14. Input the number of iterations wanted between two Fourier Transform calculations. Increasing this number will decrease computation time and increase the accuracy.
15. Input the number of discontinuities wanted along the cable as well as their values and locations along the cable.